HHS Public Access

Author manuscript

*Curr Biol*. Author manuscript; available in PMC 2023 October 10.

Published in final edited form as:

*Curr Biol*. 2022 October 10; 32(19): 4225–4239.e7. doi:10.1016/j.cub.2022.08.025.

# Parallel encoding of $CO_2$ in attractive and aversive glomeruli by selective lateral signaling between olfactory afferents

**Dhruv Zocchi**[1,2], **Emily S. Ye**[1], **Virginie Hauser**[1], **Thomas F. O' Connell**[1], **Elizabeth J. Hong**[1,*]

[1]Division of Biology & Biological Engineering, California Institute of Technology, Pasadena, CA, 91125

[2]Janelia Research Campus, Howard Hughes Medical Institute, Ashburn, VA 20147

## SUMMARY

We describe a novel form of selective crosstalk between specific classes of primary olfactory receptor neurons (ORNs) in the *Drosophila* antennal lobe. Neurotransmitter release from ORNs is driven by two distinct sources of excitation, direct activity derived from the odorant receptor and stimulus-selective lateral signals originating from stereotypic subsets of other ORNs. Consequently, the level of presynaptic neurotransmitter release from an ORN can be significantly dissociated from its firing rate. Stimulus-selective lateral signaling results in the distributed representation of $CO_2$–a behaviorally important environmental cue that directly excites a single ORN class – in multiple olfactory glomeruli, each with distinct response dynamics. $CO_2$-sensitive glomeruli coupled to behavioral attraction respond preferentially to fast changes in $CO_2$ concentration, whereas those coupled to behavioral aversion more closely follow absolute levels of $CO_2$. Behavioral responses to $CO_2$ also depend on the temporal structure of the stimulus: flies walk upwind to fluctuating, but not sustained, pulses of $CO_2$. Stimulus-selective lateral signaling generalizes to additional odors and glomeruli, revealing a subnetwork of lateral interactions between ORNs that reshapes the spatial and temporal structure of odor representations in a stimulus-specific manner.

## One Sentence Summary:

A novel subnetwork of stimulus-selective lateral interactions between primary olfactory sensory neurons enables new sensory computations.

## eTOC blurb

*Lead Contact, correspondence to ejhong@caltech.edu.

AUTHOR CONTRIBUTIONS

**Dhruv Zocchi:** Conceptualization, Methodology, Investigation, Validation, Formal analysis, Writing – Original Draft, Writing – Review & Editing, Visualization. **Emily S. Ye:** Investigation, Validation, Formal analysis. **Virginie Hauser:** Investigation, Validation. **Thomas F. O' Connell:** Methodology. **Elizabeth J. Hong:** Conceptualization, Methodology, Formal analysis, Writing – Original Draft, Writing – Review & Editing, Visualization, Supervision, Funding acquisition.



DECLARATION OF INTERESTS

The authors declare no competing interests.

Zocchi *et al*. describe a novel form of stimulus-selective crosstalk between primary olfactory neurons in *Drosophila*. The subnetwork of selective lateral interactions enables new sensory computations that can dramatically reformat the spatial and temporal structure of odor input in a stimulus-specific manner.

**Keywords**

sensory processing; primary afferents; olfactory receptor neuron; *Drosophila* ; carbon dioxide; lateral interactions; antennal lobe; temporal filtering; stimulus dynamics; odor intermittency; olfactory attraction and aversion

## INTRODUCTION

Sensory circuits share a common functional architecture in which many parallel feedforward pathways, each tuned to a specific feature of the external world, carry signals into the brain. In olfactory circuits, these parallel pathways correspond to anatomically discrete synaptic compartments called glomeruli. All olfactory receptor neurons (ORNs) expressing a given odorant receptor (OR) protein convergently project to a single glomerulus, and each second-order projection neuron (PN) receives direct input from a single glomerulus[1,2]. This orderly sorting of input, in which the glomerulus is the basic unit of information processing defined by the chemical selectivity of its cognate OR, is a hallmark of olfactory circuit organization. Most stimuli, including most odors, activate multiple receptors, and PN output reflects the integration of direct input, mediated by its cognate OR, and indirect (or lateral) input, derived from OR activity in other glomeruli. A core problem in sensory processing is to understand the computational logic of this integration, particularly the extent to which lateral interactions may or may not depend on the feature selectivity of neurons they interconnect[3,4]. This question is important because stimulus-specific interactions could serve as the substrate for many types of useful sensory computations, such as feature extraction, signal decorrelation, or logic gating.

The antennal lobe of the fruit fly, *Drosophila melanogaster*, is an experimentally tractable, numerically compact olfactory system comprising ~50 distinct glomeruli, with a similar overall circuit organization to the vertebrate olfactory bulb[5]. Lateral crosstalk between glomeruli begins in ORNs, where global GABAergic inhibition at presynaptic terminals regulates the gain of olfactory input[6,7]. In addition, a small population of excitatory local neurons mediates weak coupling between PNs[8–10]. However, in both cases, interactions between glomeruli are broad and mostly nonselective, acting to globally scale PN output proportionally to ongoing levels of overall ORN activity[11–14].

Whereas most odors broadly activate multiple ORs, some specialized odors are recognized only by a dedicated OR type. Such specialist odors are usually ethologically significant to the animal, serving as salient signals for danger, food, or reproduction[15,16]. One well-studied example is $CO_2$, an important but complex environmental cue for animals across diverse phyla[17,18]; it can signal positive or negative value, depending on context. For example, $CO_2$ is a major byproduct of microbial fermentation of organic substrates, a primary food source for *Drosophila*[19,20]. But high $CO_2$ has also been proposed to be a stress signal emitted by

conspecifics[21], or a signal of potential predators or parasites. Behavioral aversion to $CO_2$ in flies is mediated by a single chemoreceptor complex Gr63a/Gr21a, acting in the ab1C class of ORNs[21–23]. Aversion to very high concentrations of $CO_2$ also involves the acid-sensitive ionotropic receptor, Ir64a[24]. However, in certain active behavioral states, such as flight or rapid walking, flies can be attracted to $CO_2$[20,25]. This attraction is mediated by an unknown chemosensory pathway distinct from that mediating aversion[20], motivating a search for additional classes of $CO_2$-responsive ORNs.

In the course of this search, we discovered a novel form of lateral information flow between ORNs, distinct from previously described forms of global lateral connectivity, in that it acts selectively and directionally among local subnetworks of glomeruli. A consequence of this new form of lateral information flow is that neurotransmitter release from an ORN can be significantly more broadly tuned compared to its OR-mediated spiking responses. Additionally, stimulus-selective lateral signaling restructures odor responses in ORN presynaptic terminals in at least two ways – by altering the glomerular representation of odors and by reshaping the temporal dynamics of neurotransmitter release from olfactory afferents to postsynaptic targets in the brain. Using the neural processing of $CO_2$ as an example, we illustrate how novel sensory computations emerge from stimulus-selective crosstalk between olfactory afferents, and how they relate to the dependence of different olfactory behaviors on the temporal structure of odor stimuli.

## RESULTS

### ORNs in multiple glomeruli respond to $CO_2$

Using in vivo two-photon calcium imaging, we volumetrically imaged from ORN axon terminals in the antennal lobe of flies expressing the genetically encoded calcium indicator GCaMP6f[26] in all ORNs, while delivering 3 s pulses of $CO_2$ (Figure 1A, Figure S1). In addition to responses in the known class of $CO_2$-responsive ORNs (ab1C) targeting the V glomerulus[21–23], we also observed reliable, stimulus-locked calcium responses in at least three additional glomeruli – DL1, DM1, and VA2 (Figures 1A, S1A, and see Methods) – corresponding to ORN classes not previously reported as being $CO_2$-sensitive[21,27]. $CO_2$-evoked ORN responses in all four glomeruli were abolished by antennal amputation, indicating the responses are olfactory in origin (data not shown).

We initially focused on glomerulus VA2, which is easily identifiable and innervated by ab1B ORNs[27–29] (Figure 1). $CO_2$-evoked calcium signals in VA2 ORN terminals exhibited unusual response dynamics, comprised of a fast excitatory component riding on a delayed inhibitory component, both of which scaled with stimulus intensity (Figure 1B–C). The transient dynamics of the VA2 ORN response to a prolonged 10 s pulse of $CO_2$ contrasted with the sustained responses in VA2 to a 10 s pulse of diacetyl or ethyl butyrate (Figure 1D–E), odors which directly elicit spiking in ab1B ORNs (Figure 2B). Similarly, the response of ORNs in the V glomerulus to $CO_2$, which elicits spiking in V-projecting ab1C ORNs, also exhibited a typical sustained, step-like profile (Figure 1F, G). The unusual temporal dynamics of $CO_2$-evoked signals in VA2 ORNs suggested they might arise through a different mechanism.

### Modulation of $CO_2$-evoked responses in VA2

The results so far were surprising to us because prior studies using similar methods did not observe ORN responses to $CO_2$ in any glomeruli besides V[11,21]. However, $CO_2$-evoked responses in VA2 ORNs were unusual in that they were modulated in amplitude over the duration of the recording. Early in each experiment, $CO_2$ typically elicited only inhibition in VA2 ORNs, whereas at later time points, the mixed excitation and inhibition typical of a full response was observed (Figure 2A–C). The selective potentiation of the excitatory component of the VA2 $CO_2$ response was not explained by changes in the health of the preparation or other experimental artifacts, such as photobleaching, because concurrently measured $CO_2$-evoked ORN responses in V or diacetyl-evoked ORN responses in VA2 were stable over the duration of the experiment. Modulation of VA2 $CO_2$ responses did not depend on prior exposure to $CO_2$ – dissected experimental preparations that were left unstimulated for thirty minutes and then subjected to a single pulse of $CO_2$ exhibited a full potentiated response in VA2 ORNs (data not shown). Most flies (~90%) started in the "low state" dominated by inhibition, and the excitatory component began to steadily increase in amplitude typically between ten and twenty minutes after the start of the experiment (Figure S2A). Once initiated, the potentiation typically continued unabated, and most flies exhibited a stable "high state" after thirty minutes. Rarely, some flies started the experiment already in the high state or remained in the low state throughout (Figure S2B). Finally, we found that, whereas the response of VA2 ORNs to most odors was stable, responses to acetic acid and short chain fatty acids were also modulated with characteristics mirroring those of $CO_2$ (Figure 2D and data not shown). These results may explain, in part, why prior studies have not observed responses to $CO_2$ outside the V glomerulus[11,21] and further suggested that the response may arise via a different mechanism from conventional ORN responses.

### $CO_2$-evoked responses in VA2 occur in ab1B ORN terminals

We next investigated the origin of $CO_2$-evoked responses in VA2 ORNs. The cell bodies and dendrites of 2-4 classes of ORNs are housed together in stereotypical combinations within a specialized sensory structure called a sensillum[30,31]. The ab1 sensillum contains four ORN classes, ab1A-D (Figure S3A). Extracellular recordings of ab1B ORNs, which project to the VA2 glomerulus, confirmed they do not spike in response to $CO_2$[27] at any concentration from 0.5 to 10% $CO_2$ (Figure 3A–B, and data not shown). These recordings were performed in flies with ab1 A ORNs genetically ablated, to guarantee unambiguous identification of ab1B spikes (Figure 3A, Figure S3A–B). We concurrently expressed GCaMP6f in ~75% of ORNs in this fly, including ab1B, using the promoter for the insect OR co-receptor *Orco*[28,32] (Figure 3A). Neither $CO_2$ nor acetic acid elicited spiking in ab1B ORNs, but both odors evoked strong calcium responses in ORN axons in VA2 (Figure 3A–B). In single-sensillum recordings in which ab1B units were held for > 1 hour, responses to diacetyl and ethyl butyrate were stable throughout the experiment, whereas spiking responses to $CO_2$ or acetic acid were never observed (data not shown).

We considered two possible explanations for the mismatch between odor responses in ab1B ORNs recorded near the soma and at the presumptive axon terminals in VA2. First, $CO_2$-evoked responses in VA2 might not come from ab1B axon terminals, but rather from a separate class of ORNs that also projects to VA2 (Figure 3Ci, Di). Alternatively, $CO_2$-

evoked responses in VA2 do come from ab1B terminals but are driven by lateral input to ab1B from another class of ORNs that directly detects $CO_2$. To distinguish between these possibilities, we killed ab1B neurons by expressing diphtheria toxin[33] (DTI) under the control of the *Or92a* promoter while imaging from axon terminals of *Orco*-positive ORNs. Genetic ablation of ab1B ORNs resulted in a complete loss of $CO_2$-evoked responses in VA2 (Figure 3Cii–iii); odor responses in other glomeruli were unaffected (e.g. DM1, Figure 2Cii, and data not shown). Thus, responses to $CO_2$ in VA2 do not arise from non-ab1B, *Orco*-positive ORNs with terminals in VA2. In a parallel experiment, we ablated all *Orco*-positive ORNs, including ab1B ORNs, and imaged from remaining *Orco*-negative ORN terminals using a pan-ORN driver (Figure 3Di). Again, we observed no response to $CO_2$ in VA2 (Figure 3Dii–iii), although odor responses in glomeruli innervated by *Orco*-negative ORNs (e.g. glomerulus V) were unaffected (Figure 3Dii). Since all ORNs are either *Orco*-positive or *Orco*-negative, $CO_2$-evoked responses in VA2 ORNs must be occurring in the terminals of ab1B ORNs.

## The excitatory and inhibitory components of $CO_2$-evoked lateral input arise from genetically separable sources

That $CO_2$-evoked responses in VA2 occur in ab1B axon terminals, but are not driven by action potentials in ab1B ORNs, implied that ab1B terminals must receive two distinct sources of excitation: *direct* excitation from Or92a-mediated olfactory transduction, and *lateral* excitation from one or more other ORN classes. First, we confirmed that $CO_2$ responses in VA2 were indeed independent of OR function in ab1B ORNs. Because a mutation in the *Or92a* gene was not available, we functionally silenced ab1B ORNs by mutating *Orco*[32] (Figure 4A). Olfactory transduction and odor-evoked spiking in ab1B neurons were abolished in $Orco^2$ mutants (Figure 3B, 4Bi, and data not shown). Nevertheless, $CO_2$-evoked excitation in VA2 persisted in $Orco^2$ mutants, as did $CO_2$-evoked activity in glomerulus V, which is targeted by non-*Orco* dependent ab1C ORNs (Figure 4Bi–ii, S3D). However, the inhibitory component of $CO_2$-evoked activity in VA2 was lost, altering the dynamics of the $CO_2$ response in $Orco^2$ mutants (Figure 4Bi–ii, S3D). Thus, $CO_2$-evoked inhibition in ab1B terminals requires the activity of an *Orco*-dependent OR(s).

Since $CO_2$-evoked excitation in ab1B terminals does not depend on OR function in ab1B ORNs, these data imply that ab1B ORNs receive non-*Orco* dependent lateral excitation at some location between the soma and the presynaptic terminal. To determine its source, we next considered the principal sensor for $CO_2$ in flies, the Gr63a/Gr21a receptor complex acting in ab1C ORNs. $CO_2$-evoked excitation in VA2 was lost in $Gr63a^1$ mutants[22], whereas the response to diacetyl, which directly elicits spiking in ab1B ORNs (Figure 3B), was intact (Figure 4C–D, S3E). $CO_2$-evoked calcium signals in V ORNs were absent, confirming that $Gr63a^1$ renders the Gr63a/Gr21a complex non-functional. Furthermore, although the $Gr63a^1$ mutation eliminated the excitatory component of VA2 responses to $CO_2$, the inhibitory component remained (Figure 4Di–ii, S3E). These results demonstrate that the excitatory and inhibitory components of $CO_2$-driven lateral input arise from distinct receptors, and the source of $CO_2$-driven lateral excitation in ab1B ORNs is Gr63a/Gr21a.

If $CO_2$-driven excitation in VA2 depends on Gr63a/Gr21a activity in ab1C neurons, then optogenetic stimulation of ab1C ORNs should be sufficient to evoke responses in ab1B terminals. We expressed the red-shifted channelrhodopsin CsChrimson[34] in ab1C ORNs and imaged from ORN terminals in VA2, while stimulating the antennae with red light (625 nm) (Figure 4E). Light-dependent activation of ab1C ORNs (Figure S3C) evoked calcium responses in VA2, which were dependent upon raising the flies on retinal (Figure 4Fi–ii). Like responses elicited by $CO_2$, optogenetically evoked responses in VA2 ORNs also increased in amplitude over the course of the experiment (Figure 4G). Thus, ab1B terminals are activated by lateral excitation from ab1C ORNs, arguing that $CO_2$ responses in VA2 do not stem from direct or indirect effects of $CO_2$ on a secondary target.

We next conducted pharmacological and genetic experiments to investigate the synaptic mechanisms mediating $CO_2$-evoked lateral signaling. $CO_2$-evoked responses in VA2 ORNs were unaffected by pharmacological inhibition of the major neurotransmitter systems in the *Drosophila* antennal lobe: acetylcholine, GABA, or glutamate (Figure S4A–B, and data not shown). Likewise, $CO_2$-evoked activity in VA2 ORNs was unaffected by mutating *shakB*, which encodes an innexin subunit previously shown to mediate electrical coupling in the antennal lobe (Figure S4C)[10,35,36]. The only intervention that affected lateral signaling was pharmacological inhibition of the $Na^+/K^+$-ATPase by ouabain, which selectively abolished the excitatory component of $CO_2$-evoked responses (Figure S4D). The mechanism(s) by which $Na^+/K^+$-ATPase inhibition affects lateral signaling requires more investigation, but could include changes in local ionic concentrations, changes in excitability, and/or direct effects on receptors mediating intercellular communication (see Figure S4D legend).

## Lateral information flow occurs between many classes of ORNs

To determine if stimulus-selective lateral signaling occurs more generally beyond ab1B ORNs, we investigated the ab1A class of ORNs which projects to glomerulus DM1 (Figure 5A). Levels of odor-evoked spiking and odor-evoked presynaptic calcium were also decoupled in ab1A ORNs (Figure 5B). For instance, $CO_2$ and pentanol, odors that did not elicit spiking in ab1A ORNs, elicited reliable calcium signals in ab1A terminals. In $Or42b^{EY}$ mutants[37], in which olfactory transduction and odor-evoked spiking in ab1A ORNs were abolished (Figure 5D, blue), ab1A terminals in DM1 responded strongly to many odors, including $CO_2$ (Figure 5D, magenta; Figure S5A–B), and the rank order of odor response strength was changed compared to wild type (Figure 5A–D). An exception was ethyl acetate ($10^{-8}$), which did not evoke calcium responses in ab1A terminals in $Or42b^{EY}$ mutants. This observation is consistent with the selectivity of ethyl acetate ($10^{-8}$) for ab1A ORNs[12] (Figure S5A–B) and thus the lack of non-ab1A ORN activity that could be a source of lateral input. Control experiments using genetic ablation and cell-specific expression confirmed that odor-evoked lateral signals in DM1 do not reflect the misidentification of DM1 nor the detection of out-of-plane signals stemming from imperfect optical sectioning (Figure S5E–F). Notably, the amplitude of lateral signals evoked in ab1A terminals was poorly predicted by the overall level of ORN activity elicited by each stimulus (Figure S5C–D), inconsistent with a scenario where every ORN class is equivalently coupled to ab1A ORNs. Taken together, these results show that ab1A ORNs receive lateral inputs from many classes of ORNs, and this lateral signaling occurs in a glomerulus- and stimulus-selective manner.

If calcium responses in ab1A terminals arise in part from activity in other ORNs, silencing other ORNs in addition to ab1A should reduce these responses. Indeed, odor-evoked calcium signals in DM1 ORN terminals were nearly eliminated in the *Orco*$^{2}$ mutant (Figure 5E–F, magenta). An exception was the excitatory response to CO2, though, like in VA2 ORNs, the inhibitory component of $CO_2$-evoked lateral input in DM1 ORNs was also *Orco*-dependent (Figure 5F).

Finally, we investigated a third class of ORNs – the ab4A ORNs expressing Or7a and projecting to glomerulus DL5[2,28]. We imaged from ab4a terminals in DL5 in *Or7a*$^{\text{KI-Gal4/Y}}$ hemizygous flies, in which ab4A ORNs lack a functional OR (Figure 5G). As expected, stimuli that strongly excite Or7a, such as E2-hexenal and benzaldehyde[38], elicited weaker calcium responses in ab4A terminals of *Or7a*$^{\text{KI-Gal4/Y}}$ flies compared to controls. However, odors that broadly excite many ORs (e.g., ethyl butyrate) elicited strong responses in ab4A terminals in *Or7a* $^{\text{KI-Gal4/Y}}$ flies (Figure 5H); these signals must arise from OR activity in non-ab4A ORNs. These results show that ab4A ORNs, which are housed in a different olfactory sensillum from ab1A and ab1B ORNs, also receive lateral inputs that restructure presynaptic calcium responses. We conclude that stimulus-selective lateral signaling is not unique to ab1B ORNs, but rather reflects a more general feature of the circuit that extends beyond the processing of $CO_2$.

## Dual encoding of $CO_2$ in different glomeruli with distinct response dynamics

Having shown that stimulus-selective lateral signaling can reshape the spatial (glomerular) representation of odors, we next investigated its impact on the temporal dynamics of odor representations. VA2 ORN terminals responded to a long pulse of $CO_2$ with transient excitation that adapted rapidly below baseline; this adaptation was driven by the slower inhibitory component of $CO_2$-evoked lateral input that dominated with prolonged stimulation (Figures 1D, 6A). These fast-adapting dynamics were unique to ORN presynaptic calcium arising from lateral input and contrasted with non-adapting responses elicited by direct OR-mediated excitation in either VA2 (from diacetyl or ethyl butyrate) or V (from $CO_2$) ORNs (Figures 1E–F, 6B).

ORN response dynamics were transmitted to postsynaptic PNs. VA2 PN dendrites responded phasically to rapid changes in $CO_2$ concentration at the onset and offset of a sustained $CO_2$ pulse (Figure 6C) but more faithfully followed the absolute concentration of either diacetyl or ethyl butyrate (Figure 6D, data not shown). Similar results were observed in DM1 ORNs and PNs (Figure S6A–D). In response to a 1 Hz train of fluctuating $CO_2$ or ethyl butyrate, VA2 and DM1 ORN and PN responses followed the individual pulses of either odor, but encoded fluctuations of $CO_2$ fluctuations with higher contrast compared to ethyl butyrate (Figure 6A–D, Figure S6A–D). Thus, the response dynamics in a given glomerulus can depend on the chemical identity of the stimulus.

$CO_2$ signals in the natural environment span a wide range of timescales (see Discussion). We delivered $CO_2$ at varying frequencies to flies while measuring calcium signals from presynaptic ORN axons and postsynaptic PN dendrites in VA2 or V (Figure 6E, G). At low frequencies, calcium responses in V ORNs, and V PNs, more accurately followed absolute levels of $CO_2$ compared to VA2 ORNs and PNs, which adapted strongly. However,

as the stimulus frequency increased, V ORNs failed to keep pace and encoded stimulus fluctuations with decreasing contrast compared with VA2 ORNs (Figure 6E). The power spectral density estimate of the ORN or PN calcium signal in each glomerulus showed that the fractional signal power at the stimulus frequency was significantly higher for VA2 ORN or PN responses, as compared to glomerulus V, and this effect became more pronounced as the stimulus frequency increased, up to 1 Hz (Figure 6F, H). Thus, stimulus-selective lateral signaling enables the representation of $CO_2$ in different glomeruli with distinct response dynamics: ORNs and PNs in VA2 are more effective at capturing fast changes in $CO_2$ concentration, whereas V ORNs and PNs more faithfully follow slow changes in absolute $CO_2$ levels.

## The temporal structure of $CO_2$ stimuli regulates upwind walking

Given that the fly olfactory system generates parallel representations of $CO_2$ that preferentially encode fast and slow signals, we hypothesized that the temporal dynamics of $CO_2$ may be important for how flies behave towards it. To test this idea, we measured odor-dependent upwind walking in a miniature wind-tunnel environment in which well-controlled dynamic odor stimuli were delivered to the fly[39]. Starved flies were acclimated in a low-height, rectangular arena in which they were unable to fly, along the length of which flowed a constant stream of air (Figure 7A). Ten second pulses of fluctuating (0.5 Hz, 50% duty cycle) or sustained $CO_2$ were introduced at a final concentration of 5% into the airstream; photoionization detector measurements confirmed the temporal structure of the stimulus was preserved at different positions in the arena (Figure S7C–E).

Walking *Drosophila* turn upwind when they encounter attractive odors[39–41]. We observed that actively walking flies (see Methods) oriented and walked upwind in response to fluctuating, but not sustained, 5% $CO_2$ (Figure 7B, 7E–F). Upwind attraction to fluctuating $CO_2$ was comparable in strength to that towards a sustained pulse of apple cider vinegar (Figure 7C–D), a highly appetitive odor to flies[19,39]. Upwind walking at the offset of $CO_2$ stimulus also depended on the temporal structure of the stimulus – flies exhibited a prominent decrease in upwind velocity at the offset of fluctuating $CO_2$, but a transient increase in upwind velocity at the offset of sustained $CO_2$ (Figure 7E–F). However, mean groundspeed was similar during either fluctuating or sustained $CO_2$ (Figure 7J), and mean crosswind velocity was unchanged by either stimulus (Figure 7G). Changes in upwind velocity were due to the odor, rather than small mechanical stimuli associated with valve switching, since upwind velocity was unaffected in blank trials of sustained or fluctuating clean air (Figure 7C–D).

The neural mechanisms mediating attraction to $CO_2$ are unknown in *Drosophila*. We hypothesized that $CO_2$-evoked lateral input to ORNs in VA2 or DM1, glomeruli associated with olfactory attraction[40,42], may be important for upwind attraction to fluctuating $CO_2$. ORN ablations significantly reduced overall levels of walking in flies (data not shown). Thus, we turned to *Orco*$^2$ mutants, in which $CO_2$-evoked signals in VA2 and DM1 presynaptic terminals are restructured compared to wild type flies (Figure 3B). As expected, normal upwind attraction to apple cider vinegar was absent in *Orco*$^2$ mutants[25,42] (data not shown); however, like wild type flies, *Orco*$^2$ mutants oriented and walked upwind in

response to fluctuating $CO_2$ (Figure 7H–I). In contrast to wild type flies, however, *Orco*$^2$ mutants also walked upwind in the presence of sustained $CO_2$ (Figure 7H–I). Although *Orco*$^2$ mutants were less likely to be actively moving (fewer *Orco*$^2$ trials had initial groundspeed >1 mm/s, see Methods and Table S2), those that were active walked faster during the stimulus (Figure 7J).

Thus, olfactory transduction in a population of Orco-dependent ORNs is required for behavioral attraction to ACV but is dispensable for attraction to $CO_2$. We propose that $CO_2$-evoked lateral excitation, which is Orco-independent, elicits neurotransmitter release from VA2 and DM1 ORNs and activates downstream neural pathways that couple to attraction. The unexpected upwind attraction of *Orco*$^2$ but not wild type flies to sustained $CO_2$ supports this hypothesis. The behavior mirrors the persistent excitation in VA2 and DM1 ORN terminals evoked by sustained $CO_2$ in *Orco*$^2$ flies (Figure 4B, 5F), as compared to the normal transient excitation observed in wild type flies (Figure 6A, S6A–B). We propose that the restructuring of neural representations of $CO_2$, mediated by lateral signaling, in ORNs associated with behavioral attraction contributes to how flies behave differently towards $CO_2$ stimuli of varying temporal structure.

## DISCUSSION

We show that a previously undescribed form of lateral information flow, comprised of mixed excitation and inhibition between olfactory afferents, markedly reshapes the spatiotemporal structure of input odor representations in *Drosophila*. This result builds on prior observations of lateral excitatory coupling between primary sensory neurons, including invertebrate primary mechanosensory neurons, invertebrate and vertebrate photoreceptors, and primate peripheral nociceptive fibers[43–46], but is distinguished by the selectivity of lateral interactions between specific afferent inputs. We demonstrate that *Drosophila* ORN presynaptic calcium signals can be driven by two sources of excitation: 1) direct excitation derived from OR-mediated transduction, and 2) lateral input derived from stereotypic subsets of other ORNs. Thus, excitation originating from different classes of ORs is combined and processed before even leaving the primary afferents.

The selective and directional nature of the new form of lateral signaling has important consequences for odor coding. First, since stimulus-selective lateral input enters ORNs downstream of action potential generation, levels of odor-evoked neurotransmitter release can be decoupled from firing rate (Figure 3B, 5B). This fact is dramatically illustrated by strong odor-evoked calcium signals in the presynaptic terminals of functionally silent ORNs lacking an OR (Figure 5D, H). These results provide another example of unconventional neuronal integration where the axon can act as a separate computational compartment, integrating local input to control neurotransmitter release independent of activity in the soma or dendrites[47–49].

Second, stimulus-selective lateral signaling contributes to the broadening of PN odor tuning compared to their presynaptic ORNs[50,51]. PN broadening promotes the more uniform distribution and greater separability of odor representations in PN coding space. It arises from several mechanisms, including high ORN-to-PN convergence[51], depression at ORN-

PN synapses[52], and local GABAergic inhibition[6,7,12–14]. Dense electrical coupling between PNs may also boost PN responses to weak inputs[8–10]. These mechanisms act mostly uniformly across glomeruli. In contrast, glomerulus-selective lateral signaling leads to broader tuning of specific glomeruli to specific odors, which may be governed by the functional relationships among the odors (see below). Selective lateral interactions may contribute to previously observed differences in the rank order of odor preferences between cognate ORNs and PNs of the same glomerulus[50,51], which are difficult to account for by global mechanisms.

Third, stimulus-selective lateral signaling enables new synaptic computations in the antennal lobe. The interplay of lateral input with direct OR-mediated excitation modifies the dynamics of odor-evoked presynaptic calcium in a manner that depends on odor and glomerulus identity. Glomerular output dynamics can contain information about the chemical identity of the stimulus (Figure 6A–D)[4,53], and the same odorant can be represented in multiple glomeruli which each preferentially represent different temporal features of the stimulus (Figure 6E). These temporal characteristics may be matched to the requirements of different downstream behaviors to which individual glomeruli are coupled (see below).

## Mechanisms of stimulus-selective lateral signaling

Our experiments argue against a role in stimulus-selective lateral signaling for most of the well-characterized forms of synaptic signaling in the antennal lobe, including cholinergic-, GABAergic-, or glutamatergic chemical transmission or *shakB*-mediated electrical coupling (Figure S4A–D). Inhibition of the $Na^+/K^+$-ATPase pump selectively abolished the excitatory component of $CO_2$-evoked lateral inputs, potentially exerting its effects through disruption of local ionic gradients, changes in excitability, and/or direct effects on intercellular communication (see Figure S4D legend). That $CO_2$-driven lateral signals are modulated from a low to a high responsive state during the experiment may also provide an important clue about the underlying mechanism, for instance, by pointing towards a role for neuromodulation[54–56] (see Figure S2). However, we cannot rule out the possibility that the low state is a byproduct of exposing the brain, though we emphasize that conventional odor responses arising from direct ORN activity are stable in amplitude and dynamics.

A strong candidate mechanism for selective lateral ORN interactions is ephaptic coupling between ORN axons, a phenomenon observed in other unmyelinated axons[57–59] and hypothesized to occur between vertebrate olfactory afferents[60,61]. Ephaptic coupling arises from electric field effects between adjacent axons projecting through an electrically isolated extracellular space, such as occurs in nerve bundles. ORN axons with distinct cross-sectional diameters are spatially clustered in antennal nerve fascicles[62], but the reconstruction of identified ORN axons is incomplete in the fly hemibrain connectome, precluding us from evaluating the physical proximity of the axons of laterally interacting ORN classes (Figure S4F). No lateral signal flow was observed between ORNs that enter the antennal lobe through different afferent pathways, the antennal nerve and the maxillary nerve (Figure S5G), consistent with the hypothesis that adjacency between ORN axons is important for lateral signaling. A better understanding of the physical arrangement of axons assigned to

identified ORN classes in the antennal nerve may provide insight into the logic of their lateral coupling.

## The role of lateral ORN signaling in the neural processing of $CO_2$

Whereas aversive responses to $CO_2$ are known to be mediated by Gr63a/Gr21a and the V glomerulus, the mechanisms underlying attraction to $CO_2$ are less clear. Many ORNs receiving $CO_2$-evoked lateral signals correspond to glomeruli, such as VA2 and DM1, that mediate attraction to food odors like apple cider vinegar[27,42,63]. $CO_2$-mediated lateral signals in VA2 and DM1 are comprised of a fast Gr63a/Gr21a-dependent excitatory component and a slow Orco-dependent inhibitory component (Figure 4A–D). Orco-dependent inhibition is unlikely to arise from direct suppression of OR activity since $CO_2$-evoked responses in ab1A ORNs (in DM1) lacking *Or42b* exhibit pronounced inhibition (Figure 5D). Although unexpected, a role for Orco in the neural processing of $CO_2$ is supported by the altered $CO_2$-driven behavior of *Orco*$^2$ flies in walking and flight[25] (Figure 7H–I).

How does stimulus-selective lateral signaling contribute to the neural processing of $CO_2$? First, since $CO_2$ levels vary with the stage of fruit ripening and fermentation[19,20], the presence of $CO_2$ in complex natural food odors could provide information about the quality of the emitting source. For instance, $CO_2$-evoked lateral input to DM1 and VA2 ORNs (which detect small esters and ketones abundant in fruit odors) could increase the sensitivity and/or sharpen temporal responses to $CO_2$-containing food odor blends (Figure S6E–G), potentially improving the ability of these ORNs to track fast fluctuations in odors arising from fermenting sources.

Second, the encoding of $CO_2$ with distinct dynamics in multiple glomeruli, enabled by stimulus-selective lateral signaling, may contribute to how flies behave differently towards $CO_2$ of different temporal structure. We identified the temporal structure of $CO_2$ stimuli as another important variable controlling attraction to $CO_2$ (Figure 7E–F). These results build on prior work demonstrating that odor intermittency, resulting from a plume's filamentous structure, is required for upwind navigation of pheromone plumes – male moths fly upwind in response to pulsed pheromone, but not in an airstream homogeneously odorized with pheromone[64–66]. Behavioral avoidance of $CO_2$ in walking flies has been mostly observed in response to sustained increases in $CO_2$ concentration[19,21–23]. However, in both free and tethered flight, where $CO_2$ can be intermittent due to either natural plume structure or the local spatiotemporal modulation of plume structure by the wings, flies are attracted to $CO_2$[20,25].

Odor intermittency was a critical feature of early models for odor-guided navigation of natural pheromone plumes by moths[67]. Each encounter with an odor packet in the plume was proposed to evoke a phasic neural response that would be behaviorally coupled to an upwind surge, whereas a separate tonic response would activate counterturning[67]. If the phasic mechanism were dominant to the tonic mechanism, repeated brief encounters with odor would result in persistent upwind flight, but entry into homogeneous odor would lead to adaptation of the phasic mechanism and non-productive crosswind casting. The representation of $CO_2$ in multiple glomeruli with distinct response dynamics can be

interpreted in this framework (Figure S7F). We hypothesize that, in the integration of olfactory inputs by downstream circuits, activity in phasic pathways like the VA2 and DM1 glomeruli is dominant to that in the tonic V glomerulus. Fluctuating $CO_2$, which efficiently excites all $CO_2$-responsive glomeruli (Figure 6E, G), would promote upwind attraction (Figure 7E) via the dominant phasic pathways (VA2/DM1), whereas sustained $CO_2$, which only transiently excites VA2/DM1 (Figure 6A, B) but persistently activates V (Figure 1F), would promote avoidance. Consistent with this hypothesis, loss of $CO_2$-evoked inhibition in *Orco*$^2$ flies prevents adaptation of VA2 and DM1 ORN responses to $CO_2$ (Figure 4B), and *Orco*$^2$ flies walk reliably upwind in sustained $CO_2$ (Figure 7H–I). A less parsimonious but plausible alternative is that V PN responses of varying temporal dynamics couple differentially to downstream motor programs driving attraction or aversion, with an unknown *Orco*-dependent $CO_2$ input suppressing aversion during sustained stimulation. Additional investigation is required to distinguish between these models.

Subsequent work has shown that the way the temporal structure of odor stimuli influences olfactory behavior depends on odor identity. For instance, in tethered flight, the ability of *Drosophila* to track odor plumes fluctuating at different temporal frequencies differs for different odors[68]. In freely behaving flies, stimulus fluctuations are necessary for upwind attraction to $CO_2$ (Figure 7E–F), but are dispensable for attraction to apple cider vinegar or fermented banana – flies walk or fly reliably upwind in environments homogeneously odorized with these cues[39,69]. Analogously, intermittency is also required for upwind flight of mosquitoes to $CO_2$, but not for the attractive odor lactic acid (a component of human breath and skin odor)[70]. For both flies and mosquitoes, $CO_2$ is a component of important natural attractive odor sources (fermented fruit for flies or human hosts for mosquitoes), but also occurs in varied contexts in the environment. In the context of the phasic/tonic model for odor navigation, neural pathways coupled to upwind attraction may adapt differently to different attractive stimuli. As an example, odors that unambiguously signal positive value, for instance food odors like ethyl acetate, diacetyl, or ethyl butyrate (Figures 1D–G and 6A–D), would engage upwind attraction pathways (e.g., VA2 and DM1 ORNs) with little adaptation compared to a context-dependent stimulus like $CO_2$, thereby suppressing turning and driving persistent upwind movement as long as the food odor is present.

The complexity of $CO_2$ coding in the fly olfactory system likely reflects the diversity of contexts in which flies encounter $CO_2$ in the world. *Drosophila* navigating natural odor plumes in flight would experience fast fluctuating $CO_2$ emanating from a distant fermenting source[71,72]. Slower sustained $CO_2$ cues might be encountered during short range interactions with exhalations from large animals, overcrowded populations of flies or other arthropods, or dangerous enclosed natural sources of $CO_2$, such as a seeping hive or rotting log. Rapid adaptation of $CO_2$ responses in glomeruli coupled to attraction would curb attraction to potentially dangerous sources of high, persistent $CO_2$. This process may be analogous to previously proposed mechanisms for curtailing $CO_2$-evoked activity in V ORNs in the presence of food odors, which serve to enable approach to $CO_2$-emitting fermenting fruit[54,73,74].

### The roles of lateral interactions in olfactory processing

This study is one of the most direct demonstrations of selective lateral interactions between specific glomeruli in an olfactory circuit. The highly ordered organization of the antennal lobe, combined with genetic access to identified cell types, allowed the mapping of a subnetwork of preferentially connected glomeruli. In the vertebrate olfactory bulb, evidence for selective lateral interactions is mixed[4,75–78] and has focused on selective inhibition between glomeruli, inferred from anticorrelated neural activity. Recent studies suggest that inhibitory interactions between olfactory bulb glomeruli are sparse and selective, acting between glomeruli tuned to odors that do not share obvious functional relationships[76,77,79]. These observations argue against a conventional role for sparse inhibition in mediating contrast sensitivity in the olfactory bulb but leaves unanswered what functions it may serve. In the antennal lobe, selective lateral interactions are occurring via a different circuit mechanism, because they are non-GABAergic and are comprised of mixed excitation and inhibition with varying dynamics (Supplementary Figure S1). This study illustrates how, in the case of $CO_2$, selective lateral signaling reformats sensory representations to the antennal lobe in a manner that supports its coupling to an appropriate behavioral response to this important environmental cue. It may provide a useful guide for future investigations into the broader functions of selective lateral interactions in olfactory circuits.

## STAR METHODS

### Resource Availability

**Lead Contact—**Further information and requests for resources should be directed to and will be fulfilled by the Lead Contact, Elizabeth J. Hong (ejhong@caltech.edu)

**Materials Availability—**This study generated two new transgenic lines, *LexAop-DTI* (III) and *Or42a-LexA* (III). These stocks will be deposited in the Bloomington *Drosophila* Stock Center collection.

### Data and Code Availability

- All functional imaging, electrophysiology, and behavioral videos will be made available to any researcher for the purposes of reproducing or advancing the results.
- Software in this study was adapted from existing code. All custom scripts have been deposited at GitHub and are publicly available as of the date of publication. The URLs are listed in the key resources table.
- Any additional information required to reanalyze the data reported in this paper is available from the lead contact upon request.

### Experimental Model and Subject Details

*Drosophila melanogaster* were raised on a 12:12 light:dark cycle at 25°C and 70% relative humidity on cornmeal/molasses food containing: water (17.8 l), agar (136 g), cornmeal (1335.4 g), yeast (540 g), sucrose (320 g), molasses (1.64 l), $CaCl_2$ (12.5 g), sodium tartrate (150 g), tegosept (18.45 g), 95% ethanol (153.3 ml) and propionic acid (91.5 ml). All

experiments were performed in female flies 5-20 days post-eclosion, with the exception of experiments in the *shakB*$^{2}$ genotype, which were performed in hemizygous males, and behavioral experiments (see below). Complete genotypes of the flies used in each figure panel are given in Table S1.

## Method Details

**Fly stocks—**The transgenes used in this study were acquired from the Bloomington Drosophila Stock Center (BDSC), unless otherwise noted, and have been previously characterized as follows: *pebbled-Gal4* expresses Gal4 in all ORNs[80]; *Orco-LexA* was from T. Lee and expresses LexA under the control of the *Orco* promoter[81]; *Or42b-Gal4* expresses Gal4 in ab1A ORNs[29]; *Or92a-Gal4* expresses Gal4 in ab1B ORNs[29]; *Gr21-Gal4* expresses Gal4 in ab1C ORNs[28]; *GH146-Gal4* expresses Gal4 in a large subset of PNs, including DM1 and VA2 PNs[82]; *VT12760-Gal4* (III) expresses Gal4 in multiglomerular PNs with dendrites in glomerulus V[83]; *Orco*$^{2}$ has a null mutation in the *Orco* gene[32]; *Gr63a*$^{1}$ has a null mutation in the *Gr63a* gene[22]; *Or42b*$^{\mathrm{EY14886}}$ has an insertional mutation that disrupts the *Or42b* gene[84]; *shakB*$^{2}$ was from R. J. Wyman and carries a nonsense mutation in the signal sequence of shakB, rendering it a functional null[36]; *Ir25a*$^{1}$ has a null mutation in the *Ir25a* gene[85]; *UAS-opGCaMP6f* and *LexAop-opGCaMP6f* were gifts from Barret D. Pfeiffer and David J. Anderson and were used for all functional calcium imaging experiments; *UAS-CsChrimson-mVenus* expresses a Venus-tagged red-shifted channelrhodopsin[34] under Gal4 control. *UAS-DTI* and *LexAop-DTI*, which express the DTI mutant form of diphtheria toxin subunit A in a Gal4-[33] or LexA-dependent manner, respectively, were used for cell ablations.

*LexAop-DTI* flies were generated in this study by PCR amplifying the *DTI* gene from the *pUAS-DTI* plasmid[33], a gift from Leslie M. Stevens, and replacing (at the ATG) the open reading frame for *myr::GFP* in plasmid *pJFRC19-13xLexAop2-IVS-myr::GFP*[86] with that of *DTI* using isothermal assembly[87]. *pJFRC19-13xLexAop2-IVS-myr::GFP* was kindly provided by Gerald Rubin (Addgene plasmid #26224). The final sequence of the construct was confirmed by Sanger sequencing, and transgenic flies were generated by site-specific integration of *LexAop-DTI* into the attP2 landing site (BestGene, Inc., Chino Hills, CA).

*Or42a-LexA* flies were generated as follows. The *Or42a* promoter was PCR amplified from a bacterial artificial chromosome (RPCI-98 library, clone 45O18, BACPAC Resources) containing the *Or42a* locus of *D. melanogaster* using primers[28]:

5’-CCGGTACACTAAAACGAACCGTAAACC-3’

5’-TGCACTCTAATTTCAACAATTGAACTAAAGCA -3’.

The *Or42a* promoter was inserted 5’ to *nlsLexA::p65* using isothermal assembly in vector *pBPnlsLexA::p65Uw*, replacing the ccdB cassette. The plasmid *pBPnlsLexA::p65Uw* was kindly provided by G. Rubin (Addgene plasmid #26230, RRID:Addgene_26230). The final sequence of the construct was confirmed by Sanger sequencing, and transgenic flies were generated by site-specific integration into the VK27 landing site on chromosome III (BestGene, Inc., Chino Hills, CA). To examine the selectivity of the driver, *Or42a-LexA* was crossed to *13xLexAop2-mCD8:gfp* (RRID:BDSC_32205), and brains of the resulting

progeny flies (2 days old) were dissected and immunostained with antibodies directed against GFP and nc82. GFP expression was observed in pb1A ORN axons in the VM7 glomerulus. Some off-target expression was also observed in glomeruli VL2p and V, but these glomeruli were easily distinguishable from VM7 in imaging experiments based on their position.

**Odor Delivery—**Odors were delivered essentially as previously described[11]. The olfactometers used for odor stimulus delivery are diagrammed in Figure S7A–B. For all odors except $CO_2$, a constant stream of air (200 ml/min) was directed at the fly. Ten percent of the airstream (20 ml/min) was routed through the "normally open" port of a three-way solenoid valve (ASCO 411-L-1324-HVS, NISCO, Inc., Duluth, GA) and passed through the headspace of a control vial filled with solvent, before rejoining the main carrier stream. When triggered by an external valve command, the three-way valve redirected the 20 ml/min odor stream to exit through the "normally closed" port and into the headspace of the vial filled with odor. The 20 ml/min control or odor streams were carried by tubing of matched lengths and rejoined the carrier stream at the same point along the carrier tube, approximately 10 cm from the fly. Thus, the concentration of odor in the vial headspace for all odors was diluted by a factor of 10 in air. The exceptions were acetic acid, which was diluted 2-fold, and ammonia, which was diluted 100-fold, in air. Odor concentrations are reported as the v/v dilution of odor in paraffin oil (J.T. Baker, VWR #JTS894) in the vial, with the exceptions of ammonia and acetic acid, which were diluted in water.

For delivery of $CO_2$, the olfactometer was modified such that the odor stimulus line and the control balance line were each controlled by their own 3-way solenoid valve. The stimulus line exited from the "normally closed" port of its valve (the "normally open" port of that valve was vented outside the microscope box). The balance line exited from the "normally open" port of its valve (the "normally closed" port of that valve was vented outside the microscope box). Flow rates in the stimulus and balance lines were always equal, and stimulus line and balance line valves each received the same external command signal. The stimulus and balance lines each joined a constant carrier stream of air (180 ml/min) at the same point along the carrier tube (Figure S7A), approximately 10-cm from the end of the tube. In this way, the total flow rate experienced by the fly was kept constant. For instance, for the delivery of a 5% $CO_2$ stimulus, the olfactometer functioned as follows. Under default (non-stimulus) conditions, the balance line, carrying 10 ml/min of air, joined the carrier stream, carrying 190 ml/min of air, to direct a total of 200 ml/min of air at the fly; the 10 ml/min of 100% $CO_2$ in the stimulus line was vented. When the command signal was high, the stimulus line, carrying 10 ml/min of 100% $CO_2$, joined the carrier stream, carrying 190 ml/min of air, to direct a total of 200 ml/min of 5% $CO_2$ at the fly; the 10 ml/min of air in the balance line was vented. $CO_2$ stimuli of varying concentration were generated by adjusting the relative flow rates of the carrier line (from 180 to 199 ml/min), and the stimulus and balance lines (from 1-20 ml/min).

For either olfactometer, the opening of the carrier tube measured 4 mm in diameter and was positioned approximately 1 cm from the fly. A small funnel (10-cm diameter) connected to a vacuum line was placed behind the fly to vent odors. Flow rates were metered using mass flow controllers (MC series, Alicat Scientific, Tucson, AZ), and all air was first passed

through a charcoal filter before being routed into the mass flow controllers. Odor blends (Figure S6E–G) were generated by mixing in air. A total flow rate of 200 ml/min at the fly was used for all experiments, except for the optogenetic experiments in Figure 4E–G and the experiments in Figures 6 and S6, where a total flow rate of 2 L/min was used. In Figure 4E–G, the flow rate was increased to reduce the latency of the odor stimulus to better match the short latency of the light stimulus. In Figure 6, a higher flow rate was used to reduce low-pass filtering of rapidly fluctuating odor stimuli.

**Two-photon calcium imaging—**In vivo functional calcium imaging was performed essentially as previously described[11]. After a brief period of cold anesthesia (<20 s), the fly was head-fixed, the dorsal cuticle was removed, and the antennal lobes were exposed. The antennae were snugly secured below the imaging chamber, keeping them dry and responsive to odors. Antennal lobes were imaged from the dorsal side; horizontal imaging planes were acquired at varying depths along the dorsal-ventral axis of the antennal lobes, spaced approximately ~10 μm apart.

In experiments where we amputated antennae or palps, the third segment of the antennae or the palps of restrained flies were bilaterally removed with a pair of sharp forceps, under the visual control of a dissecting microscope. Flies were allowed to recover for fifteen minutes before the head capsule was opened to prepare for imaging.

Two-photon GCaMP6f fluorescence was excited with 925 nm light from a Mai Tai DeepSee laser (Spectra-Physics, Santa Clara, CA). Images were acquired with an Olympus 20X/1.0 numerical aperture objective (XLUMPLFLN20XW) on a two-photon microscope equipped with galvo-galvo scanners (Thorlabs Imaging Systems, Sterling, VA) at 5.5 frames $s^{-1}$ at a resolution of 224x224 pixels covering an area of 90 x 90 $\mu m^2$ (Figures 1 and 2) or 140 x 140 $\mu m^2$ (all other data). The collection filter was centered at 525 nm with a 50 nm bandwidth, with the exception of the optogenetic experiments (see below). The microscope was housed in a lightproof box, and experiments were conducted at room temperature (~22°C). The brain was constantly perfused by gravity flow with saline containing (in mM): 103 NaCl, 3 KCl, 5 N-Tris(hydroxymethyl)methyl-2-aminoethane-sulfonic acid, 8 trehalose, 10 glucose, 26 $NaHCO_3$, 1 $NaH_2PO_4$, 1.5 $CaCl_2$, and 4 $MgCl_2$ (pH 7.3, osmolarity adjusted to 270– 275 mOsm). The saline was bubbled with 95% $O_2$/5% $CO_2$ and circulated in the bath at ~2-3 ml $min^{-1}$.

Specific glomeruli were identified using a combination of their anatomical depth, location, size, and shape in the baseline fluorescence signal, which are invariant across flies. Their identity was confirmed by evaluating their characteristic odor response properties, using a test panel of odors presented at relatively low concentration (spanning $10^{-4}$ to $10^{-8}$). For experiments in Figure 1 where we surveyed for glomeruli that are responsive to $CO_2$, the antennal lobe of many flies (>10 flies) was systematically sampled at 5μm intervals all along the entire depth of the antennal lobe while repeatedly presenting $CO_2$ to the fly. Glomeruli exhibiting reliable $CO_2$-evoked calcium activity across all individuals (DL1, DM1, VA2, V) were then identified using the above criteria.

Imaging trials were 30 s each, with the stimulus delivered 10s after the onset of imaging. The response to a given stimulus was measured as a block of three replicate trials, and stimulus blocks were delivered in pseudo-random order. The intertrial interval was 3 s. For experiments in Figures 3C–D; 4, 5, and S5, recordings from experimental and control flies were interleaved. The experimenter was not blind to the condition. Odor-evoked responses (including $CO_2$-evoked responses) were indistinguishable between wildtype flies and flies carrying one balancer chromosome (*SM6* or *TM6B*). Balancer chromosomes only appear in control genotypes in functional imaging experiments (e.g., the heterozygous control, see Table S1) and are necessarily present if sibling flies (arising from the same instance of a parental cross) are to be directly compared.

When collecting odor-evoked responses for each stimulus-glomerulus pair, the average amount of time elapsed from the start of the experiment to the measurement was matched between genotypes. This matching was done to ensure that any differences observed between genotypes was not due to systematic differences in the time course of the modulation of $CO_2$-evoked responses in VA2 ORNs. The only exception to this was for a small subset of *Gr63a*$^1$ flies, from which we recorded $CO_2$-evoked responses in VA2 ORNs two hours after the start of the experiment, to account for the possibility that the mutation may simply delay the conversion of the response. Excitatory responses of VA2 ORNs to $CO_2$ were never observed, although strong responses to diacetyl were present.

**Optogenetics—**For the experiments in Figure 4E–G, flies were raised on cornmeal/molasses food supplemented with one teaspoon of potato flakes rehydrated 1:1 (v/v) with 140 μM all-trans retinal in water. All-trans-retinal was prepared as a 35 mM stock in ethanol and stored at −20°C. The parental cross that generated experimental flies was carried out in the dark on all-trans-retinal-supplemented medium, and newly eclosed experimental flies were maintained in the dark, also on all-trans-retinal medium, until used in experiments.

Calcium imaging of optogenetically evoked signals was performed essentially as described above with the following modifications. The collection filter for imaging was centered at 500 nm with a 20 nm bandwidth (HPX500-20, Newport Corporation, Irvine, CA). The use of this filter allowed simultaneous detection of GCaMP6f fluorescence emission while stimulating with red light, without stimulus bleed-through to the detector. Light was delivered from the tip of an optical fiber (400-μm core, 0.39 NA, Thorlabs, Newton, NJ) butt-coupled to a 625nm LED (M625F2, 1000 mA, Thorlabs, Newton, NJ). The tip of the optical fiber was positioned ~ 1 mm away from the antennae, which were tucked beneath the stainless steel floor of the imaging chamber.

Odor and light stimulus trials were interleaved during the experiment. A 1 s pulse of light was used for optogenetic stimulation. This pulse duration was chosen based on the results of pilot single-sensillum recordings of light-evoked firing rates in ab1C ORNs in the flies (which express CsChrimson in ab1C ORNs and GCaMP6f in *Orco*-positive ORNs, Figure 4E). Light pulses of greater than 1 s duration resulted in ORNs firing a short burst of spikes (~250 ms) and subsequently entering into depolarization block.

**Pharmacology—**All drugs were bath applied in the saline. Mecamylamine was used at 100 μM. Picrotoxin and CGP54626 were used at 5 μM and 50 μM, respectively. Oubain was used at 100 μM. Drugs were washed-in for 5 min before initiating recordings.

**Single-sensillum Recordings—**Single-sensillum recordings were performed essentially as previously described[51]. Briefly, flies were immobilized in the end of a trimmed pipette tip, and one antenna was visualized under a 50x air objective. The antenna was stabilized by tightly sandwiching it between a set of two fine glass hooks, fashioned by gently heating pipettes pulled from glass capillaries (World Precision Instruments, TW150F-3). A reference electrode filled with saline (see above) was inserted into the eye, and a sharp saline-filled glass recording microelectrode was inserted into the base of the sensillum. ab1sensilla were identified based on their characteristic size and morphology, position on the antenna, and the presence of four distinct spike waveforms (in wild type flies), each having a characteristic odor sensitivity[27] (see also Figure S3). Signals were acquired with a MultiClamp 700B amplifier, low-pass filtered at 2 kHz, and digitized at 10 kHz. Delivery of odor- and light-stimuli was carefully matched to that in functional imaging experiments. To unambiguously distinguish ab1A from ab1B spikes in some critical experiments, it was necessary to kill one of these ORN types using diphtheria toxin expression (Figure S3A–B and Figures 3A–B and 5A–B).

**Measuring $CO_2$-evoked neural responses—**$CO_2$-evoked responses in ORNs in glomeruli VA2 and DM1 generally converted over the course of a recording from a “low” state, dominated by inhibition, to a “high” state, characterized by mixed excitation and inhibition (Figure 2). In separate experiments, we found that this modulation of the $CO_2$ response does not require prior odor exposure and can be observed with just two presentations of $CO_2$, one measured immediately after the fly is placed on the recording rig and one measured thirty minutes later (data not shown).

The fact that the time course of the modulation of the $CO_2$ response could vary significantly across different flies (Figure S2) presented a challenge to defining the “early” and “late” response. In a typical experiment, including the experiments in Figure 2A–C, the “early” response of all glomeruli of interest to all stimuli of interest was measured within the first five minutes after placing the fly on the rig. The response of ORNs in VA2 was then periodically probed by delivering $CO_2$ to the fly every ~5-10 min, until an excitatory response was observed, was stable in amplitude over multiple consecutive presentations, and > 30 min had elapsed since the start of the experiment. At this point, the response of all glomeruli to all stimuli was measured again and defined as the “late response.”

Rarely, a fly responded to $CO_2$ with a mixed excitatory/inhibitory response on the very first presentation of $CO_2$ (Figure S2B, green trace). More typically, the duration of the full conversion of the $CO_2$ response ranged from ~10-60 min. The $CO_2$ response in VA2 ORNs converted to the “high” state in almost all flies. A similar protocol was used for measuring the modulation of the response to acetic acid in VA2 ORNs (Figure 2D). In Figures 1 and 3–6, whenever possible, responses were collected from preparations that achieved the conditions we have defined as the late response; if the experimental genotype did not allow this, responses were collected at a time >30 minutes from the start of the recording. When

comparing between paired control and experimental genotypes (e.g., Figures 3 and 4), the average amount of time elapsed from the start of the experiment to the measurement of each glomerulus-stimulus pair was roughly matched between genotypes (see above). In experiments where no response was observed in the population of interest (e.g., Figure 3C–D), a subset of recordings was maintained for > 1 hour to confirm that responses were abolished and not just delayed.

$CO_2$-evoked responses in ORN terminals in glomerulus DM1 are also modulated over the course of a recording. Although we have not studied it systematically, we observed that the modulation of $CO_2$ responses in DM1 ORNs does not necessarily occur concurrently with that in VA2 ORNs.

We also considered the hypothesis that the modulation of $CO_2$-evoked calcium signals in VA2 ORN terminals originates from modulation of spiking activity in ab1B ORNs, which project to VA2. Thus, we investigated whether the spiking response of ab1B ORNs to $CO_2$ might change over the duration of an experiment, converting from unresponsive to responsive. In the sensillum recordings in Figure 3A, flies were restrained and positioned on the rig for >60 min prior to recording. We implemented this waiting period to allow for any potential conversion of ab1B responses to $CO_2$; however, ab1B ORNs were never observed to spike in response to $CO_2$. These experiments suggest that the modulation of $CO_2$-evoked calcium signals in VA2 ORN terminals does not arise from changes in ab1B spiking activity, which is also consistent with other experiments demonstrating that they have a lateral origin.

The lability of $CO_2$-evoked ORN activity is notable in the context of the state-dependent effects of $CO_2$ on fly behavior[88]. Flies behave differently in response to $CO_2$ depending on their satiety state, circadian state, temperature, and walking speed[20]. Recording ORN responses in flies behaving towards $CO_2$ will be important to linking the modulation of $CO_2$ responses with the animals' ongoing behavioral state.

**Behavioral measurements of odor-dependent upwind walking—**Upwind walking in the presence of odor was measured as previously described in a miniaturized wind tunnel apparatus constructed from sheets of laser-cut plastic[39]. In brief, the position of the fly was tracked while it walked freely in a low height (~1.7 mm), two-dimensional arena. Each individual behavioral arena had dimensions 140 mm x 40 mm, and the complete apparatus contained four arenas, allowing the behavior of four flies to be measured in parallel in each experimental run. The arena was illuminated from below with an array of infrared LEDs (850 nm), delivered through a white plastic diffuser, and imaged from above, using a monochrome Flea3 USB3.0 camera (Point Grey (now FLIR), FL3-U3-13S2M-CS).

All air was charcoal-filtered and humidified prior to introduction into the arena via an array of inlets at the upwind end of the arena. Flow rates were controlled using mass flow controllers (Alicat). A carrier line of 1.0 L/min air was joined by either a 0.4 L/min odorized line (during stimulus delivery) or a 0.4 L/min air line (as a balance in the absence of stimuli), for a total flow rate of 1.4 L/min, split equally across the four arenas. Stimulus delivery in each arena was independently controlled by a pair of fast-switching three-way solenoid valves (LHDA1233115H, The Lee Company, Westbook, CT). For each pair of

valves, only one valve (odorized or air) was open to the arena inlet at any given moment in time; the other (closed) valve was diverted to a vacuum line for venting. The odorized line or the balance line entered immediately downstream of the carrier inlet and upstream of the manifold at the upwind end of the chamber. For 1% ACV, the odorized line was passed through the headspace of a 20-ml glass vial filled with 10 ml of 1% apple cider vinegar diluted in water. For 5% $CO_2$, upstream mass flow controllers delivered 17.5% $CO_2$ to the constantly odorized line, for a final concentration of 5% $CO_2$ in the arena. Relative odor concentrations at different points in the arena were measured using a photoionization detector (miniPID, Aurora Systems, Aurora, Canada). The detector tip was stabilized at different positions in the arena through a special ceiling fabricated for these measurements. PID measurements to characterize the odor stimulus in the behavioral arena were made using 100% ethanol and showed that odor stimuli travel as an odor front down the length of the arena (Figure S7C–E).

Behavioral experiments were conducted in female flies, 2-5 days old. Wildtype flies were from a Heisenberg Canton-S stock (*HCS*). *Orco*$^2$ flies were backcrossed to wildtype *HCS* for five generations[20]; we independently confirmed the genotype by PCR. Flies were starved in an empty bottle with a moist tissue for a total of ~20-24 hours prior to the start of the experiment. Experiments were conducted in darkness at the flies' subjective dusk (between ~ZT11 and ZT12). Flies were taken from the incubator at ~ZT10, briefly cold-anesthetized (<10 s), loaded into the apparatus, and acclimated in the arena with clean air flowing for ~80-120 min prior to initiating the experiment.

Odor stimuli were of 10 s duration, with approximately ~120 s between successive stimuli. Each experiment comprised ~60-70 trials, lasting 125-140 min. Imaging and stimulus delivery were controlled by custom ROS software (https://github.com/ejhonglab/nagel_laminar). Video was recorded at a frame rate of 7 Hz.

## Quantification and Statistical Analysis

**Two photon functional imaging.—**Imaging analysis was performed in MATLAB (Mathworks, Natick, MA) using custom scripts. Regions of interest (ROIs) defining specific glomeruli were manually drawn in each imaging plane from the movie of raw fluorescence signal, using anatomical position, size, shape, and odor tuning criteria, as described above. Calcium transients (ΔF/F) were measured as changes in fluorescence (ΔF) normalized to the mean fluorescence during the baseline period (F, averaged in the 10 s prior to stimulus onset). All imaging data was background subtracted (using the mean pixel intensity outside the antennal lobe) prior to analysis. In each experiment, the calcium response in an ROI was computed as the mean across three trials of each stimulus. Unless otherwise indicated, the mean calcium responses reported in the figures are averaged across independent replicates of each experiment and represent the mean ± s.e.m. computed across flies. The *n* for each figure are in Table S1.

To generate heatmaps of peak responses in individual flies, ΔF/F was calculated on a pixel-by-pixel basis, and three consecutive frames centered on the peak of the response were averaged. For each stimulus, data were pooled by averaging the peak odor-evoked heat map

(ΔF/F) across three trials. A Gaussian low-pass filter of size 5 x 5 pixels was applied to ΔF/F maps.

**Single-sensillum recordings.—**Spikes were detected using custom scripts in MATLAB. Peristimulus time histograms (PSTHs) were computed by counting the number of spikes in 50-ms bins that overlapped by 25 ms. Single-trial PSTHs were baseline subtracted (using the spontaneous firing rate in the pre-stimulus period) and averaged together across five trials for each stimulus to generate the PSTH describing the response to an odor in a given experiment. The mean PSTHs shown in the Figures 3B and 5B, D, F represent the mean ± s.e.m. computed across multiple flies. The *n* for each figure panel are listed in Table S1.

**Behavioral experiments.—**Walking trajectories were extracted with a modified implementation (https://github.com/ejhonglab/multi_tracker) of Multi tracker, a ROS package for tracking objects in 2D[20]. Flies typically cycle between bouts of activity and inactivity throughout the day. To focus on actively moving flies, we analyzed only trials in which flies walked at a mean groundspeed >1 mm/s in the ten seconds immediately preceding stimulus onset, as in previous studies[39].

Analyses of behavioral data were performed using custom scripts in MATLAB. The *x*- and *y*-pixel coordinates of each fly at each time point was converted to mm. For each time point, we computed (1) the distance moved (in mm) as the length of the hypotenuse between *xy*-coordinates at successive time points; (2) the groundspeed (in mm/s) as the distance moved divided by the time step (~143 ms); and (3) the *x*- or *y*-velocity (in mm/s) as the *x*- or *y*-displacement, respectively, between coordinates at successive time points divided by the time step. We arbitrarily designated upwind as $y>0$, downwind as $y<0$, rightward as $x>0$, and leftward as $x<0$. Trials were discarded if they met any of the following criteria: 1) contained missing values arising from tracking errors (fewer than 1% of trials were affected by this condition); 2) more than 10% of *xy*-coordinates during the 10 s preceding the stimulus and during the 10 s stimulus were <2.5 mm away from any wall; 3) moved less than 25 mm during the entire trial; and 4) had a mean groundspeed less than or equal to 1 mm/s during the 10 s preceding the onset of the stimulus. Flies with fewer than ten trials passing these criteria were discarded. These exclusion criteria were implemented to minimize the influence of the arena's boundaries on behavior and to restrict our analyses to active flies only. The total number of flies and trials for each condition is provided in Supplemental Table S2.

**Statistical analyses.—**The number of replicates for each condition in each experiment is reported in Table S1. The number *n* represents the number of individual flies in which each measurement was made. Sample sizes were not predetermined using a power analysis. We used sample sizes comparable to those used in similar types of studies[8,21,74]. The experimenter was not masked to experimental condition or genotype during data collection and analysis.

Error bars in figures are either standard error of the mean (s.e.m.) or bootstrapped 95% confidence intervals, computed using bootci in MATLAB. Statistics were computed in MATLAB using the ranksum (Mann-Whitney U test) or kruskalwallis (Kruskal-Wallis one-

way analysis of variance by ranks) functions. For data in Figure 7, permutation testing was used to evaluate statistical differences between experimental groups because of its robustness to the effects of outliers. For each two-way comparison, observations from flies in the two experimental groups were combined and randomly reassigned (permuted) into two groups, maintaining the number of observations in each comparison group, and the difference between the means of the shuffled groups was computed. This permutation process was repeated for a total of 100,000 resamplings, and the two-tailed *p*-value for the comparison was computed as the proportion of resamplings in which the absolute difference of the resampled means was larger than the absolute value of the observed difference between experimental groups, *p*-values reported in all figures were Bonferroni corrected for multiple comparisons within a given experiment. Comparisons noted as "not significant" (n.s.) were not significant at a level of $\alpha$=0.05 after correction for multiple comparisons. The specific statistical test used for each comparison is reported in the figure legends.

## Supplementary Material

Refer to Web version on PubMed Central for supplementary material.

## ACKNOWLEDGMENTS

We are grateful to B. D. Pfeiffer and D. J. Anderson for gifts of unpublished fly stocks. We thank T. Lee, and R. J. Wyman for sharing fly stocks, and we thank G. Rubin and L. M. Stevens for sharing plasmids. We thank A. Dea for the generation of the *LexAop-DTI* flies and M. Lobb-Rabe for the generation of *Or42a-LexA* flies. We thank A. Matheson and K. Nagel for design files and advice on establishing the miniature wind tunnel walking assay. We thank F. van Breugel for help with implementing the Multi tracker package for tracking flies. We thank M. Meister, P. W. Sternberg, members of the Hong lab, and anonymous reviewers for their careful readings of the manuscript and their many insightful comments that improved this study. We especially acknowledge F. van Breugel and M. H. Dickinson for stimulating conversations and for sharing unpublished results which partially motivated this study. This work was funded by grants to E. J. H. from the NSF/CIHR/DFG/FRQ/UKRI-MRC Next Generation Networks for Neuroscience Program (NeuroNex Award #2014217), the National Institutes of Health (1U01MH109147), and the Shurl and Kay Curci Foundation. E. J. H. is a Chen Scholar of the Tianqiao and Chrissy Chen Institute for Neuroscience and a Clare Boothe Luce Professor of the Henry Luce Foundation.

## REFERENCES

1. Buck LB (1996). Information coding in the vertebrate olfactory system. Annual Review of Neuroscience 19, 517–44.
2. Vosshall LB, and Stocker RF (2007). Molecular architecture of smell and taste in Drosophila. Annu Rev Neurosci 30, 505–33. [PubMed: 17506643]
3. Isaacson JS, and Scanziani M (2011). How inhibition shapes cortical activity. Neuron 72, 231–43. [PubMed: 22017986]
4. Laurent G (1999). A systems perspective on early olfactory coding. Science 286, 723–8. [PubMed: 10531051]
5. Wilson RI, and Mainen ZF (2006). Early events in olfactory processing. Annual Review of Neuroscience 29, 163–201.
6. Root CM, Masuyama K, Green DS, Enell LE, Nassel DR, Lee CH, and Wang JW (2008). A presynaptic gain control mechanism fine-tunes olfactory behavior. Neuron 59, 311–21. [PubMed: 18667158]
7. Olsen SR, and Wilson RI (2008). Lateral presynaptic inhibition mediates gain control in an olfactory circuit. Nature 452, 956–60. [PubMed: 18344978]
8. Shang Y, Claridge-Chang A, Sjulson L, Pypaert M, and Miesenbock G (2007). Excitatory local circuits and their implications for olfactory processing in the fly antennal lobe. Cell 128, 601–12. [PubMed: 17289577]

9. Olsen SR, Bhandawat V, and Wilson RI (2007). Excitatory interactions between olfactory processing channels in the Drosophila antennal lobe. Neuron 54, 89–103. [PubMed: 17408580]
10. Yaksi E, and Wilson R.l. (2010). Electrical coupling between olfactory glomeruli. Neuron 67, 1034–47. [PubMed: 20869599]
11. Hong EJ, and Wilson RI (2015). Simultaneous encoding of odors by channels with diverse sensitivity to inhibition. Neuron 85, 573–89. [PubMed: 25619655]
12. Olsen SR, Bhandawat V, and Wilson RI (2010). Divisive normalization in olfactory population codes. Neuron 66, 287–99. [PubMed: 20435004]
13. Silbering AF, and Galizia CG (2007). Processing of odor mixtures in the Drosophila antennal lobe reveals both global inhibition and glomerulus-specific interactions. J. Neurosci 27, 11966–77. [PubMed: 17978037]
14. Silbering AF, Okada R, Ito K, and Galizia CG (2008). Olfactory information processing in the Drosophila antennal lobe: anything goes? The Journal of neuroscience : the official journal of the Society for Neuroscience 28, 13075–87.
15. Depetris-Chauvin A, Galagovsky D, and Grosjean Y (2015). Chemicals and chemoreceptors: ecologically relevant signals driving behavior in Drosophila. Front. Ecol. Evol 3.
16. Andersson MN, Löfstedt C, and Newcomb RD (2015). Insect olfaction and the evolution of receptor tuning. Front. Ecol. Evol 3.
17. Guerenstein PG, and Hildebrand JG (2008). Roles and Effects of Environmental Carbon Dioxide in Insect Life. Annual Review of Entomology 53, 161–178.
18. Jones W (2013). Olfactory Carbon Dioxide Detection by Insects and Other Animals. Mol Cells 35, 87–92. [PubMed: 23456329]
19. Faucher C, Forstreuter M, Hilker M, and de Bruyne M (2006). Behavioral responses of Drosophila to biogenic levels of carbon dioxide depend on life-stage, sex and olfactory context. J Exp Biol 209, 2739–48. [PubMed: 16809465]
20. van Breugel F, Huda A, and Dickinson MH (2018). Distinct activity-gated pathways mediate attraction and aversion to CO 2 in Drosophila. Nature 564, 420–424. [PubMed: 30464346]
21. Suh GS, Wong AM, Hergarden AC, Wang JW, Simon AF, Benzer S, Axel R, and Anderson DJ (2004). A single population of olfactory sensory neurons mediates an innate avoidance behaviour in Drosophila. Nature 431, 854–9. [PubMed: 15372051]
22. Jones WD, Cayirlioglu P, Kadow IG, and Vosshall LB (2007). Two chemosensory receptors together mediate carbon dioxide detection in Drosophila. Nature 445, 86–90. [PubMed: 17167414]
23. Kwon JY, Dahanukar A, Weiss LA, and Carlson JR (2007). The molecular basis of CO2 reception in Drosophila. PNAS 104, 3574–3578. [PubMed: 17360684]
24. Ai M, Min S, Grosjean Y, Leblanc C, Bell R, Benton R, and Suh GS (2010). Acid sensing by the Drosophila olfactory system. Nature 468, 691–5. [PubMed: 21085119]
25. Wasserman S, Salomon A, and Frye MA (2013). Drosophila Tracks Carbon Dioxide in Flight. Current Biology 23, 301–306. [PubMed: 23352695]
26. Chen TW, Wardill TJ, Sun Y, Pulver SR, Renninger SL, Baohan A, Schreiter ER, Kerr RA, Orger MB, Jayaraman V, et al. (2013). Ultrasensitive fluorescent proteins for imaging neuronal activity. Nature 499, 295–300. [PubMed: 23868258]
27. de Bruyne M, Foster K, and Carlson JR (2001). Odor coding in the Drosophila antenna. Neuron 30, 537–52. [PubMed: 11395013]
28. Couto A, Alenius M, and Dickson BJ (2005). Molecular, anatomical, and functional organization of the Drosophila olfactory system. Current Biology 15, 1535–47. [PubMed: 16139208]
29. Fishilevich E, and Vosshall LB (2005). Genetic and functional subdivision of the Drosophila antennal lobe. Current Biology 15, 1548–53. [PubMed: 16139209]
30. Shanbhag SR, Muller B, and Steinbrecht RA (1999). Atlas of olfactory organs of Drosophila melanogaster. 1. Types, external organization, innervation, and distribution of olfactory sensilla. International Journal of Insect Morphology and Embryology 28, 377–397.
31. Shanbhag SR, Müller B, and Steinbrecht RA (2000). Atlas of olfactory organs of Drosophila melanogaster: 2. Internal organization and cellular architecture of olfactory sensilla. Arthropod Structure & Development 29, 211–229. [PubMed: 18088928]

32. Larsson MC, Domingos AI, Jones WD, Chiappe ME, Amrein H, and Vosshall LB (2004). Or83b encodes a broadly expressed odorant receptor essential for Drosophila olfaction. Neuron 43, 703–14. [PubMed: 15339651]
33. Han DD, Stein D, and Stevens LM (2000). Investigating the function of follicular subpopulations during Drosophila oogenesis through hormone-dependent enhancer-targeted cell ablation. Development 127, 573–83. [PubMed: 10631178]
34. Klapoetke NC, Murata Y, Kim SS, Pulver SR, Birdsey-Benson A, Cho YK, Morimoto TK, Chuong AS, Carpenter EJ, Tian Z, et al. (2014). Independent optical excitation of distinct neural populations. Nature methods 11, 338–46. [PubMed: 24509633]
35. Phelan P (2005). Innexins: members of an evolutionarily conserved family of gap-junction proteins. Biochimica et Biophysica Acta (BBA) - Biomembranes 1711, 225–245. [PubMed: 15921654]
36. Krishnan SN, Frei E, Swain GP, and Wyman RJ (1993). Passover: A gene required for synaptic connectivity in the giant fiber system of Drosophila. Cell 73, 967–977. [PubMed: 8500183]
37. Bellen HJ, Levis RW, He Y, Carlson JW, Evans-Holm M, Bae E, Kim J, Metaxakis A, Savakis C, Schulze KL, et al. (2011). The Drosophila Gene Disruption Project: Progress Using Transposons With Distinctive Site Specificities. Genetics 188, 731–743. [PubMed: 21515576]
38. Hallem EA, and Carlson JR (2006). Coding of odors by a receptor repertoire. Cell 125, 143–60. [PubMed: 16615896]
39. Álvarez-Salvado E, Licata AM, Connor EG, McHugh MK, King BM, Stavropoulos N, Victor JD, Crimaldi JP, and Nagel KI (2018). Elementary sensory-motor transformations underlying olfactory navigation in walking fruit-flies. eLife 7, e37815. [PubMed: 30129438]
40. Bell JS, and Wilson RI (2016). Behavior Reveals Selective Summation and Max Pooling among Olfactory Processing Channels. Neuron 91, 425–438. [PubMed: 27373835]
41. Steck K, Veit D, Grandy R, Badia SBI, Badia SBI, Mathews Z, Verschure P, Hansson BS, and Knaden M (2012). A high-throughput behavioral paradigm for Drosophila olfaction - The Flywalk. Sci Rep 2, 361. [PubMed: 22511996]
42. Semmelhack JL, and Wang JW (2009). Select Drosophila glomeruli mediate innate olfactory attraction and aversion. Nature 459, 218–23. [PubMed: 19396157]
43. Bloomfield SA, and Völgyi B (2009). The diverse functional roles and regulation of neuronal gap junctions in the retina. Nature Reviews Neuroscience 10, 495–506. [PubMed: 19491906]
44. van Hateren JH (1986). Electrical coupling of neuro-ommatidial photoreceptor cells in the blowfly. J. Comp. Physiol 158, 795–811. [PubMed: 3016255]
45. Meyer RA, Raja SN, and Campbell JN (1985). Coupling of action potential activity between unmyelinated fibers in the peripheral nerve of monkey. Science 227, 184–187. [PubMed: 3966152]
46. Rabinowitch I, Chatzigeorgiou M, and Schafer WR (2013). A Gap Junction Circuit Enhances Processing of Coincident Mechanosensory Inputs. Current Biology 23, 963–967. [PubMed: 23707432]
47. Bucher D, Thirumalai V, and Marder E (2003). Axonal Dopamine Receptors Activate Peripheral Spike Initiation in a Stomatogastric Motor Neuron. J. Neurosci 23, 6866–6875. [PubMed: 12890781]
48. Liu C, Cai X, Ritzau-Jost A, Kramer PF, Li Y, Khaliq ZM, Hallermann S, and Kaeser PS (2022). An action potential initiation mechanism in distal axons for the control of dopamine release. Science 375, 1378–1385. [PubMed: 35324301]
49. Sheffield MEJ, Best TK, Mensh BD, Kath WL, and Spruston N (2011). Slow integration leads to persistent action potential firing in distal axons of coupled interneurons. Nat Neurosci 14, 200–207. [PubMed: 21150916]
50. Wilson RI, Turner GC, and Laurent G (2004). Transformation of olfactory representations in the Drosophila antennal lobe. Science 303, 366–70. [PubMed: 14684826]
51. Bhandawat V, Olsen SR, Schlief ML, Gouwens NW, and Wilson RI (2007). Sensory processing in the Drosophila antennal lobe increases the reliability and separability of ensemble odor representations. Nature Neuroscience 10, 1474–82. [PubMed: 17922008]
52. Kazama H, and Wilson RI (2008). Homeostatic matching and nonlinear amplification at genetically-identified central synapses. Neuron 58, 401–13. [PubMed: 18466750]

53. Uchida N, Poo C, and Haddad R (2014). Coding and Transformations in the Olfactory System. Annual Review of Neuroscience 37, 363–385.
54. Su C-Y, and Wang JW (2014). Modulation of neural circuits: how stimulus context shapes innate behavior in Drosophila. Current Opinion in Neurobiology 29, 9–16. [PubMed: 24801064]
55. Root CM, Ko KI, Jafari A, and Wang JW (2011). Presynaptic Facilitation by Neuropeptide Signaling Mediates Odor-Driven Food Search. Cell 145, 133–144. [PubMed: 21458672]
56. Ko KI, Root CM, Lindsay SA, Zaninovich OA, Shepherd AK, Wasserman SA, Kim SM, and Wang JW (2015). Starvation promotes concerted modulation of appetitive olfactory behavior via parallel neuromodulatory circuits. eLife 4, e08298.
57. Faber DS, and Pereda AE (2018). Two Forms of Electrical Transmission Between Neurons. Front. Mol. Neurosci 11.
58. Katz B, and Schmitt OH (1940). Electric interaction between two adjacent nerve fibres. The Journal of Physiology 97, 471–488. [PubMed: 16995178]
59. Arvanitaki A (1942). Effects evoked in an axon by the activity of a contiguous one. Journal of Neurophysiology 5, 89–108.
60. Bokil H, Laaris N, Blinder K, Ennis M, and Keller A (2001). Ephaptic Interactions in the Mammalian Olfactory System. J. Neurosci 21, RC173–RC173. [PubMed: 11588203]
61. Blinder KJ, Pumplin DW, Paul DI, and Keller A (2003). Intercellular interactions in the mammalian olfactory nerve. Journal of Comparative Neurology 466, 230–239. [PubMed: 14528450]
62. Venkatesh S, and Naresh Singh R (1984). Sensilla on the third antennal segment of Drosophila melanogaster meigen (Diptera : Drosophilidae). International Journal of Insect Morphology and Embryology 13, 51–63.
63. Faucher CP, Hilker M, and Bruyne M. de (2013). Interactions of Carbon Dioxide and Food Odours in Drosophila: Olfactory Hedonics and Sensory Neuron Properties. PLOS ONE 8, e56361. [PubMed: 23457557]
64. Baker TC, Willis MA, Haynes KF, and Phelan PL (1985). A pulsed cloud of sex pheromone elicits upwind flight in male moths. Physiological Entomology 10, 257–265.
65. Mafra-Neto A, and Cardé RT (1994). Fine-scale structure of pheromone plumes modulates upwind orientation of flying moths. Nature 369, 142–144.
66. Vickers NJ, and Baker TC (1994). Reiterative responses to single strands of odor promote sustained upwind flight and odor source location by moths. PNAS 91, 5756–5760. [PubMed: 11607476]
67. Baker TC (1990). Upwind flight and casting flight: complementary phasic and tonic systems used for location of sex pheromone sources by male moth. In Proc. 10th Int. Symp. Olfaction and Taste, Oslo, 1990, pp. 18–25.
68. Krishnan P, Duistermars BJ, and Frye MA (2011). Odor identity influences tracking of temporally patterned plumes in Drosophila. BMC neuroscience 12, 62. [PubMed: 21708035]
69. Budick SA, and Dickinson MH (2006). Free-flight responses of Drosophila melanogaster to attractive odors. Journal of Experimental Biology 209, 3001–17. [PubMed: 16857884]
70. Geier M, Bosch OJ, and Boeckh J (1999). Influence of odour plume structure on upwind flight of mosquitoes towards hosts. Journal of Experimental Biology 202, 1639–1648. [PubMed: 10333509]
71. Murlis J, Elkinton JS, and Carde RT (1992). Odor plumes and how insects use them. Annual Review of Entomology 37, 505–532.
72. van Breugel F, and Dickinson MH (2014). Plume-Tracking Behavior of Flying Drosophila Emerges from a Set of Distinct Sensory-Motor Reflexes. Current Biology 24, 274–286. [PubMed: 24440395]
73. Su C-Y, Menuz K, Reisert J, and Carlson JR (2012). Non-synaptic inhibition between grouped neurons in an olfactory circuit. Nature 492, 66–71. [PubMed: 23172146]
74. Turner SL, and Ray A (2009). Modification of CO2 avoidance behaviour in Drosophila by inhibitory odorants. Nature 461, 277–81. [PubMed: 19710651]

75. Aungst JL, Heyward PM, Puche AC, Karnup SV, Hayar A, Szabo G, and Shipley MT (2003). Centre-surround inhibition among olfactory bulb glomeruli. Nature 426, 623–9. [PubMed: 14668854]
76. Economo MN, Hansen KR, and Wachowiak M (2016). Control of Mitral/Tufted Cell Output by Selective Inhibition among Olfactory Bulb Glomeruli. Neuron 91, 397–411. [PubMed: 27346531]
77. Fantana AL, Soucy ER, and Meister M (2008). Rat olfactory bulb mitral cells receive sparse glomerular inputs. Neuron 59, 802–14. [PubMed: 18786363]
78. Luo M, and Katz LC (2001). Response correlation maps of neurons in the mammalian olfactory bulb. Neuron 32, 1165–79. [PubMed: 11754845]
79. Zavitz D, Youngstrom IA, Borisyuk A, and Wachowiak M (2020). Effect of Interglomerular Inhibitory Networks on Olfactory Bulb Odor Representations. J. Neurosci 40, 5954–5969. [PubMed: 32561671]
80. Sweeney LB, Couto A, Chou YH, Berdnik D, Dickson BJ, Luo L, and Komiyama T (2007). Temporal target restriction of olfactory receptor neurons by Semaphorin-1a/PlexinA-mediated axon-axon interactions. Neuron 53, 185–200. [PubMed: 17224402]
81. Lai SL, and Lee T (2006). Genetic mosaic with dual binary transcriptional systems in Drosophila. Nature Neuroscience 9, 703–9. [PubMed: 16582903]
82. Stocker RF, Heimbeck G, Gendre N, and de Belle JS (1997). Neuroblast ablation in Drosophila P[GAL4] lines reveals origins of olfactory interneurons. Journal of Neurobiology 32, 443–56. [PubMed: 9110257]
83. Lin H-H, Chu L-A, Fu T-F, Dickson BJ, and Chiang A-S (2013). Parallel Neural Pathways Mediate CO2 Avoidance Responses in Drosophila. Science 340, 1338–1341. [PubMed: 23766327]
84. Bellen HJ, Levis RW, Liao G, He Y, Carlson JW, Tsang G, Evans-Holm M, Hiesinger PR, Schulze KL, Rubin GM, et al. (2004). The BDGP Gene Disruption Project: Single Transposon Insertions Associated With 40% of Drosophila Genes. Genetics 167, 761–781. [PubMed: 15238527]
85. Benton R, Vannice KS, Gomez-Diaz C, and Vosshall LB (2009). Variant ionotropic glutamate receptors as chemosensory receptors in Drosophila. Cell 136, 149–62. [PubMed: 19135896]
86. Pfeiffer BD, Ngo TT, Hibbard KL, Murphy C, Jenett A, Truman JW, and Rubin GM (2010). Refinement of tools for targeted gene expression in Drosophila. Genetics 186, 735–55. [PubMed: 20697123]
87. Gibson DG, Young L, Chuang R-Y, Venter JC, Hutchison CA, and Smith HO (2009). Enzymatic assembly of DNA molecules up to several hundred kilobases. Nature Methods 6, 343–345. [PubMed: 19363495]
88. Bräcker LB, Siju KP, Varela N, Aso Y, Zhang M, Hein I, Vasconcelos ML, and Grunwald Kadow IC (2013). Essential Role of the Mushroom Body in Context-Dependent CO2 Avoidance in Drosophila. Current Biology 23, 1228–1234. [PubMed: 23770186]

## Highlights

- Lateral signaling between specific subsets of ORNs reformats odor representations.
- Levels of neurotransmitter release from ORNs can be dissociated from firing rate.
- $CO_2$ is encoded in attractive and aversive ORNs with distinct response dynamics.
- Behavioral responses towards $CO_2$ depend on the temporal structure of the stimulus.

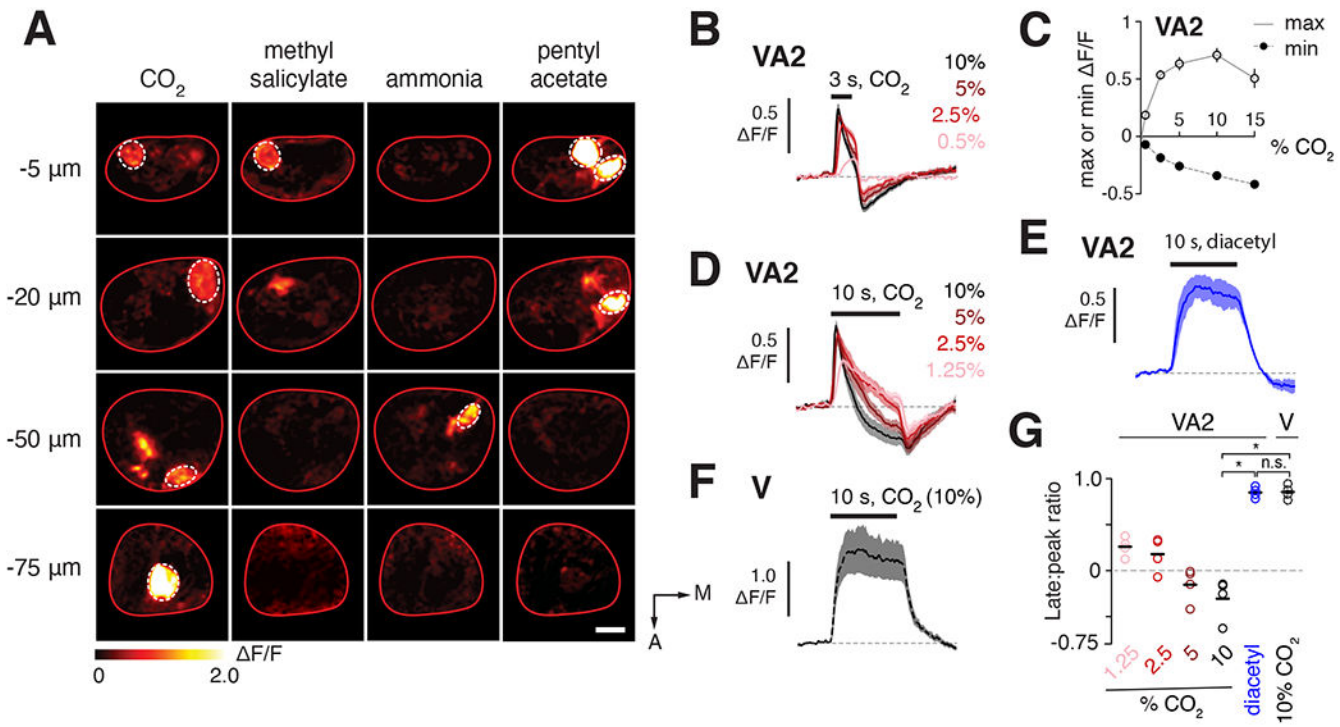


**Figure 1: $CO_2$ elicits mixed excitatory and inhibitory signals in multiple classes of ORNs.**

**A)** Representative peak ΔF/F heat maps of odor-evoked, two-photon calcium signals in ORN axon terminals in the antennal lobe (red outline). A, anterior. M, medial. Scale bar, 20µm. Each row is a different imaging plane. Dashed lines indicate $CO_2$-sensitive glomeruli and landmark glomeruli used for imaging plane identification. Stimuli are 5% $CO_2$, pentyl acetate ($10^{-5}$), $NF_4$ (10%), methyl salicylate ($10^{-5}$). **B)** Time course of change in fluorescence (mean and s.e.m.) of ORN terminals in VA2 to a 3 s $CO_2$ pulse of varying concentrations of (*n*=3-9). See also Figure S1. **C)** Mean (and s.e.m.) of maximum and minimum responses in **B. D)** Same as **B)** for a 10 s $CO_2$ stimulus (*n*=4). **E-F)** Time course of change in fluorescence (mean and s.e.m.) in VA2 ORN terminals to diacetyl ($10^{-6}$) (**E,** *n*=4) or V ORN terminals to 10% $CO_2$ (**F,** *n*=4). **G)** Mean ratio (black bar) of the amplitude of the late response (at 8s) to the peak response in **D-F.** Open circles, individual experiments. The late/peak ratios of $CO_2$ responses are negatively correlated with stimulus intensity ($R^2$=0.6053, *p*=0.0004, slope=−0.0657 with 95% CI [−0.09612, −0.03529]). **p*<0.05, repeated-measures ANOVA with Bonferroni multiple comparison; n.s., not significantly different.

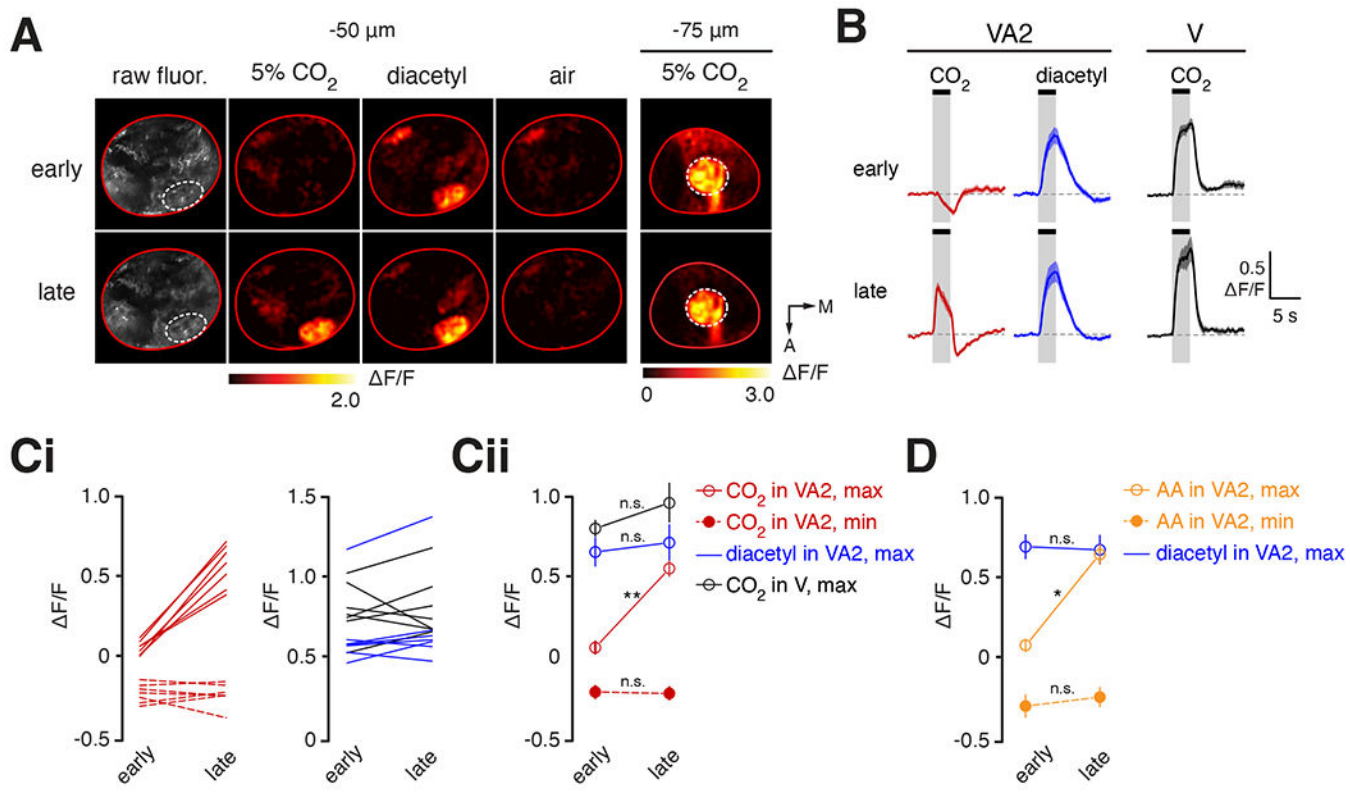


**Figure 2: $CO_2$ responses convert from a low to a high state over the course of a recording.**

**A)** Representative heat maps showing peak ORN calcium responses to 5% $CO_2$, diacetyl ($10^{-6}$), and air (control) in glomerulus VA2 or V. The first column is resting fluorescence. A, anterior. M, medial. Scale bar, 20 µm. Top, response <5 min from initiation of the experiment; bottom, same imaging field ~20 minutes later. **B)** Time course (mean and s.e.m.) of ΔF/F response in ORN terminals to $CO_2$ (VA2, red; V, black) or diacetyl (VA2, blue) at early (~1- 5 min) and late (>30 min) time points ($n$=7). **Ci)** Maximum (solid) and minimum (dashed) ORN responses in VA2 to $CO_2$ (red) or diacetyl (blue), and in V to $CO_2$ (black). Lines connect early and late measurements from the same fly (see also Figure S2). **Cii)** Mean and s.e.m. of maximum (open circles) and minimum (solid circles) responses ($n$=7). **D)** Same as **Cii**, for VA2 ORN responses to 3% acetic acid (orange) or diacetyl (blue) ($n$=5). *$p$<0.05, **$p$<0.01, two-tailed Mann-Whitney $U$-test with Bonferroni multiple-comparisons test; n.s., not significantly different.

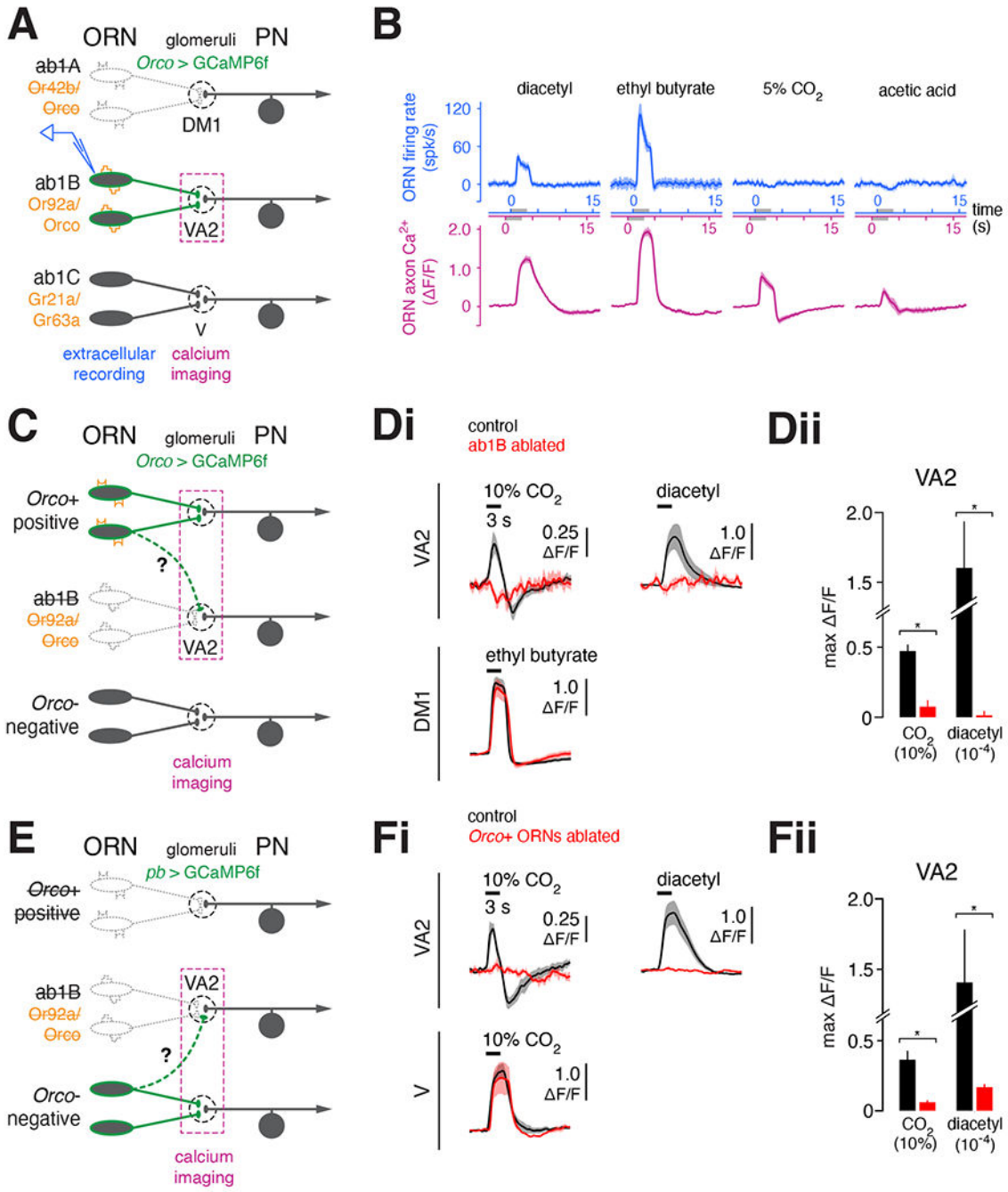


**Figure 3: $CO_2$-evoked calcium signals in VA2 occur in ab1B ORN terminals and are dissociable from ab1B spiking.**

**A, C, E)** Schematics of experimental setups. Cell ablations were achieved using cell-specific expression of diphtheria toxin (see also Table S1, Figure S3). All panels show mean and s.e.m. **B)** Comparison of peristimulus time histograms of odor-evoked ab1B spiking (blue, $n$=4-6) and odor-evoked changes in fluorescence of ORN terminals in VA2 (magenta, $n$=3-5). Odors: diacetyl ($10^{-6}$), ethyl butyrate ($10^{-4}$), 5% $CO_2$, 3% acetic acid. **Di)** Odor-evoked changes in fluorescence in *Orco*-positive ORN terminals in flies with ab1B ORNs

ablated (red, $n$=4) or intact (black, $n$=7). Odors: 10% $CO_2$, diacetyl ($10^{-4}$), ethyl butyrate ($10^{-4}$). **Dii)** Peak odor-evoked ΔF/F from **Di. Fi)** Odor-evoked changes in fluorescence in ORN terminals in flies with *Orco*-positive ORNs ablated (red, $n$=3) or intact (black, $n$=6). **Fii)** Peak odor-evoked ΔF/F from **Fi.** *$p$<0.05, two-tailed Mann-Whitney $U$-test with Bonferroni multiple-comparisons test.

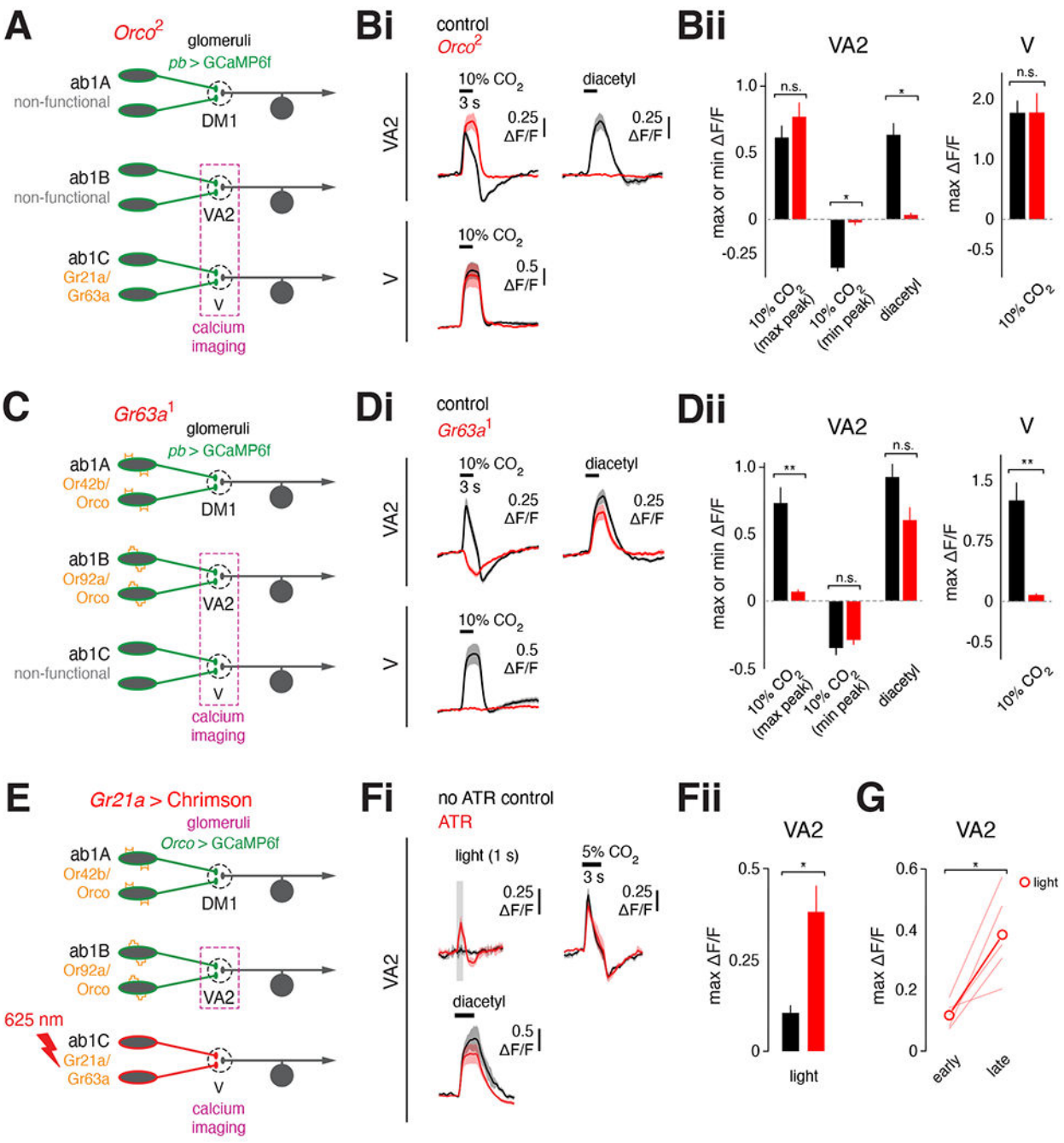


**Figure 4: $CO_2$-evoked calcium signals in VA2 are driven by lateral input from distinct, genetically separable sources.**

**A, C, E)** Schematics of experimental setups. All panels show mean and s.e.m. **Bi)** Odor-evoked calcium response in ORN terminals in VA2 or V in control (*Orco*$^2$*/TM6B,* black, $n$=4) and *Orco*$^2$ null (red, $n$=7) flies. See also Figure S3. **Bii)** Mean maximum or minimum evoked ΔF/F from **Bi. Di)** Odor-evoked calcium response in ORN terminals in VA2 or V in control (*Gr63*$^1$*/TM6B*, black, $n$=6) and *Gr63a*$^1$ null (red, $n$=7) flies. **Dii)** Mean maximum or minimum evoked ΔF/F from **Di. Fi)** Calcium signals in VA2 ORNs evoked by 1 s

light pulse (625 nm) in flies raised on food without (control, black, $n$=3) or supplemented with (ATR, red, $n$=4-5) all-*trans*-retinal. Responses of VA2 ORNs to odors are given for comparison. **Fii)** Maximum of light-evoked response from **Fi. G)** Maximum light-evoked responses in VA2 ORNs (from flies on ATR) at early and late time points in the experiment, as defined in Figure 2B. Measurements ($n$=5) from the same fly are connected. Open circles mark the mean. *$p$<0.05, **$p$<0.01, two-tailed Mann-Whitney $U$-test with Bonferroni multiple-comparisons test, n.s., not significantly different. See also Figure S4.

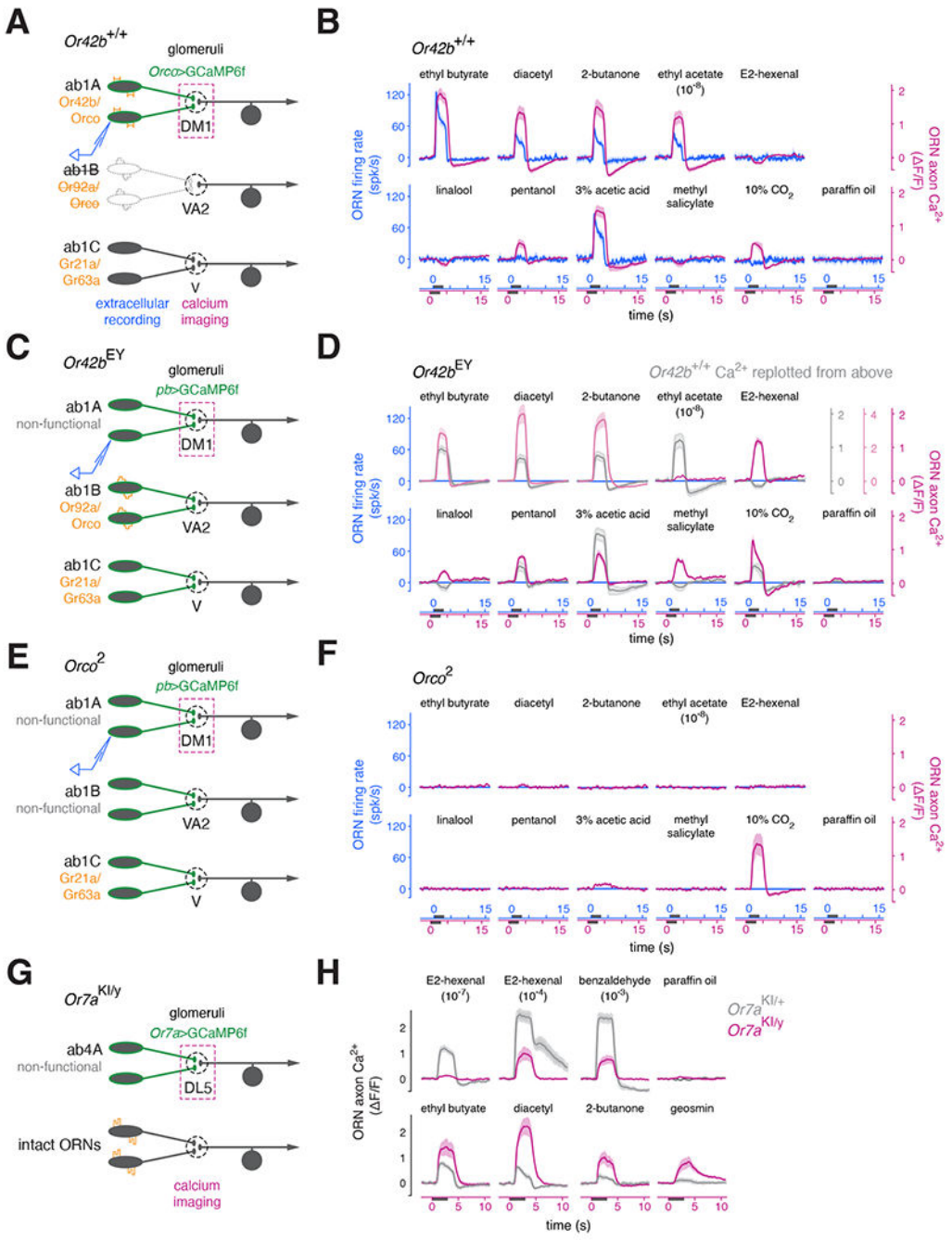


**Figure 5: Odor representations in ab1A and ab4A ORN terminals are restructured by stimulus-selective lateral signaling.**

**A, C, E, G)** Schematics of experimental setups. Odors were presented at $10^{-4}$ dilution, except where otherwise indicated. All responses are mean and s.e.m. **B)** Peristimulus time histograms (PSTHs) of odor-evoked ab1A spiking (blue, $n$=3) or changes in fluorescence (ΔF/F) in ab1A ORN terminals in DM1 (magenta, $n$=4-11) in control flies. Time axes for calcium responses in **B**, **D**, and **F** are forward shifted to visually align the onset of the two types of responses. **D)** Same as **B** for *Or42b*$^{EY}$ null flies (blue, ab1A firing rate, $n$=3;

magenta, calcium response in ab1A terminals in DM1, *n*=6-13). Calcium responses from control flies (from **B**) are overlaid (grey) for reference. See also Figure S5. **F)** Same as **B** for *Orco*$^{2}$ null flies (blue, PSTH of ab1A firing rates, *n*=3; magenta, calcium response in ab1A terminals in DM1, *n*=3-5). **H)** Odor-evoked calcium responses in ab4A terminals in DL5 in control (*Or7a*$^{\text{Gal4-KI/+}}$ heterozygous, grey, *n*=4-6) or *Or7a*$^{\text{Gal4-KI/Y}}$ hemizygous null (magenta, *n*=4-5) flies.

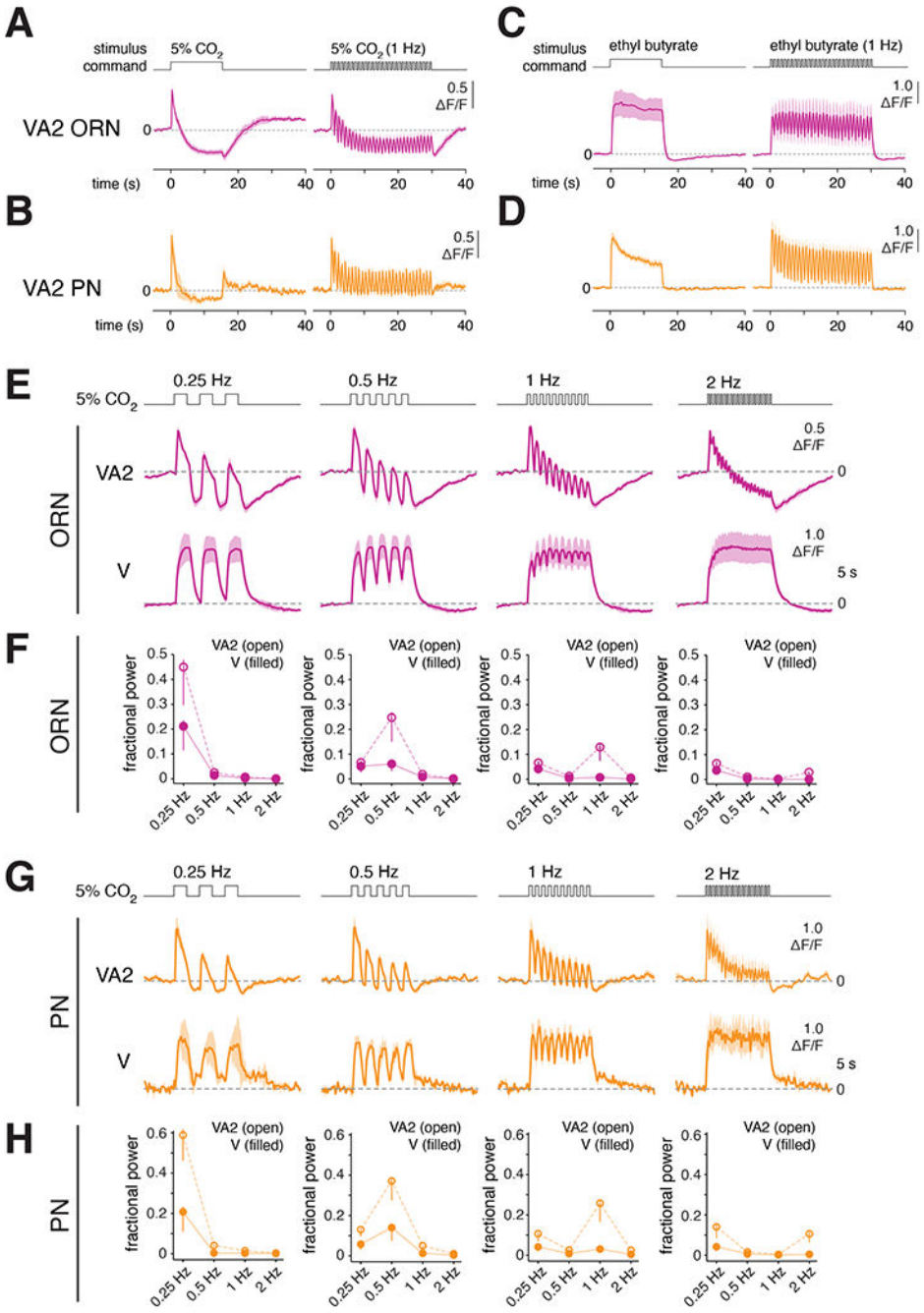


**Figure 6: Lateral signaling between ORNs results in odor- and glomerulus-specific response dynamics that are transmitted to PNs.**

**A-B)** Calcium responses in VA2 ORN axon terminals (**A**, magenta, $n$=4 flies) or VA2 PN dendrites (**B**, orange, $n$=5-7 flies) to a sustained 15 s pulse of 10% $CO_2$ (left) or a 30 s 1 Hz train of 10% $CO_2$, pulsed at 50% duty cycle. Top row, odor valve command. **C-D)** Same as **A-B**, but in response to ethyl butyrate ($10^{-4}$). See also Figure S6. **E)** Calcium signals in ORN terminals in VA2 or V in response to a 10 s train of 10% $CO_2$ stimuli presented at 0.25 Hz, 0.5 Hz, 1 Hz, or 2 Hz, pulsed at 50% duty cycle ($n$=3). **F)** Mean fractional power at

each indicated frequency, computed from the power spectral density estimate of the calcium signals above each plot. Error bars are calculated from the 95% confidence bounds of the power spectral density estimate. **G-H)** Same as **E-F**, for PN dendrites in glomerulus VA2 or V ($n$=4 for VA2, $n$=3 for V). All calcium traces are mean and s.e.m.

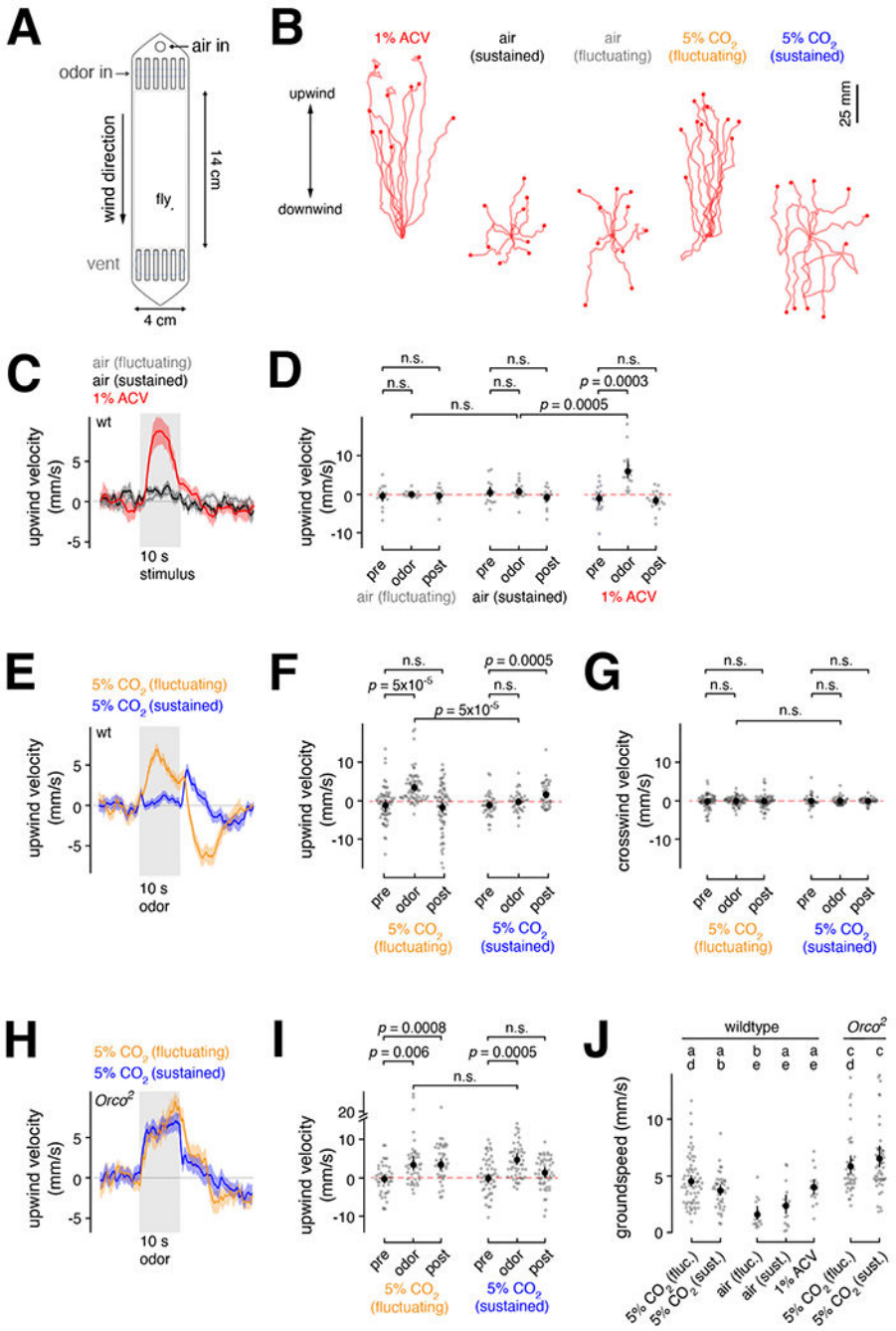


**Figure 7: Upwind walking in $CO_2$ depends on the temporal structure of the odor stimulus.**

**A)** Schematic of an individual behavioral arena (top view); one fly is sampled per arena per experiment. See also Figure S7. **B)** Ten example trajectories from a representative fly for each odor, aligned to the fly's starting position (+) at stimulus onset. Solid symbol, position at stimulus offset. **C)** Time course (mean and s.e.m.; n = 16-17 flies; see Table S2) of upwind velocity (positive values indicate y-displacement towards the odor source) in wildtype (*HCS*) flies in response to fluctuating air (0.5 Hz, 50% duty cycle), a sustained pulse of air, or a sustained pulse of apple cider vinegar (1% ACV). Shaded grey, 10-s

stimulus epoch. **D)** Mean upwind velocity for each fly in **C** in the 10-s epoch prior (pre), during (odor), and after (post) the stimulus. Grey symbol, individual mean; black symbol, group mean; error bars, bootstrapped 95% C.I. of group mean. Statistical comparisons were made by permutation testing of the difference between group means (see Methods), *p*-values were Bonferroni corrected for multiple comparisons, n.s., not significantly different ($p>0.01$). **E, H)** Same as **C** for wildtype **(E)** or $Orco^2$ **(H)** flies responding to fluctuating (0.5 Hz, 50% duty cycle) or sustained 5% $CO_2$ (n=41-69 flies/condition; see Table S2). **F, I)** Same as **D,** for each fly in **E** and **H,** respectively. **G)** Same as **F** for crosswind velocity (x-displacement) of wildtype flies in fluctuating or sustained $CO_2$. **J)** Mean groundspeed during the 10-s stimulus for all odors. The letters indicate statistically significant groups (Kruskal-Wallis test, with post-hoc Dunn test for multiple comparisons); groups sharing a letter are not significantly different ($\alpha=0.01$).

## KEY RESOURCES TABLE

| REAGENT or RESOURCE | SOURCE | IDENTIFIER |
|---|---|---|
| **Chemicals, Peptides, and Recombinant Proteins** | | |
| paraffin oil | J.T. Baker | VWR #JTS894 |
| methyl salicylate | Sigma | Cat# M6752 |
| ammonia | Pure Bright | N/A |
| pentyl acetate | Sigma | Cat # 109584 |
| diacetyl (2,3-butanedione) | Sigma | VWR #AAAA14217-09 |
| acetic acid | | |
| ethyl butyrate | Sigma | Cat #E15701 |
| 2-butanone | Sigma | Cat #360473 |
| ethyl acetate | Sigma | Cat #58958 |
| E2-hexenal | Fisher Sci | Cat #AC158131000 |
| linalool | Sigma | Cat #AC158131000 |
| pentanol | Sigma | Cat #138975 |
| all-*trans* retinal | Sigma | Cat #R2500 |
| **Critical Commercial Assays** | | |
| ZR Tissue & Insect DNA MiniPrep | Zymo | D6016 |
| **Experimental Models: Organisms/Strains** | | |
| *pebbled-Gal4* | Bloomington *Drosophila* Stock Center | RRID:BDSC_80570 |
| *Orco-LexA* | Tzumin Lee at Janelia Research Campus | N/A |
| *Or42b-Gal4* | Bloomington *Drosophila* Stock Center | RRID:BDSC_9971 |
| *Or92a-Gal4* | Bloomington *Drosophila* Stock Center | RRID:BDSC_23139 |
| *GH146-Gal4* | Bloomington *Drosophila* Stock Center | RRID:BDSC_30026 |
| *VT12760-Gal4* (III) | Vienna *Drosophila* Resource Center | RRID:SCR_200022 |
| $Orco^{2}$ | Bloomington *Drosophila* Stock Center | RRID:BDSC_23130 |
| $Gr63a^{1}$ | Bloomington *Drosophila* Stock Center | RRID:BDSC_9941 |
| $Or42b^{EY14886}$ | Bloomington *Drosophila* Stock Center | RRID:BDSC_20956 |
| $Or7a^{KI\text{-}Gal4}$ | Bloomington *Drosophila* Stock Center | RRID:BDSC_91810 |
| $shakB^{2}$ | Robert Wyman at Yale University | N/A |
| *UAS-opGCaMP6f* | Barret Pfeiffer and David Anderson at Caltech | N/A |
| *LexAop-opGCaMP6f* | Barret Pfeiffer and David Anderson at Caltech | N/A |
| *UAS-CsChrimson-mVenus* | Bloomington *Drosophila* Stock Center | RRID:BDSC_55135 |
| *UAS-DTI* | Bloomington *Drosophila* Stock Center | RRID:BDSC_25039 |
| *LexAop-DTI* | This paper | N/A |
| *Gr21-Gal4* | Bloomington *Drosophila* Stock Center | RRID: BDSC_24147 |
| $Ir25a^{1}$ | Bloomington *Drosophila* Stock Center | RRID: BDSC_41736 |
| **Recombinant DNA** | | |

| REAGENT or RESOURCE | SOURCE | IDENTIFIER |
|---|---|---|
| *pUAS-DTI* | Leslie M. Stevens, University of Texas, Austin | N/A |
| *pJFRC19-13xlexAop2-IVS-myr::GFP* | Gerald Rubin, Janelia Research Campus | RRID:Addgene_26224 |
| **Software and Algorithms** | | |
| FIJI | NIH Image | https://imagej.nih.gov/ij/ |
| Matlab R2021b | Mathworks, Natick, MA | https://www.mathworks.com/products/matlab.html |
| Adobe Illustrator | Adobe Inc., San Jose, CA | https://www.adobe.com/products/illustrator.html |
| Custom ROS software for control of behavioral assays | GitHub | https://github.com/ejhonglab/nagel_laminar |
| Custom modification of Multi tracker for extraction of walking trajectories | GitHub | https://github.com/ejhonglab/multi_tracker |